

1 ***Increasingly seasonal jet stream drives stormy episodes with joint wind-flood risk in Great Britain***

2  
3  
4  
5  
6  
7  
8  
9  
10  
11  
12  
13  
14  
15  
16  
17  
18  
19  
20  
21  
22  
23  
24  
25  
26  
27  
28  
29  
30  
31  
32  
33

John K. Hillier<sup>1</sup>, Hannah C. Bloomfield<sup>2</sup>, Colin Manning<sup>2</sup>, Freya Garry<sup>3</sup>, Len Shaffrey<sup>4,5</sup>, Paul Bates<sup>6,7</sup>, Dhirendra Kumar<sup>4</sup>.

<sup>1</sup> Dept. Geography and Environment, Loughborough University, Loughborough, LE11 3TU, UK

<sup>2</sup> School of Engineering, Newcastle University, Newcastle Upon Tyne NE1 7RU, United Kingdom

<sup>3</sup> Met Office, Fitzroy Road, Exeter, EX1 3PB, UK

<sup>4</sup> Department of Meteorology, University of Reading, Whiteknights Road, Reading RG6 7BE, United Kingdom

<sup>5</sup> National Centre for Atmospheric Science, University of Reading, Whiteknights Road, Reading RG6 7BE, United Kingdom

<sup>6</sup> School of Geographical sciences, University of Bristol, Bristol BS8 1SS, United Kingdom

<sup>7</sup> Cabot Institute, University of Bristol, University Road, Bristol BS8 1SS, United Kingdom

This is a paper that has not yet been peer reviewed, submitted to EarthArXiv.

Submitted to the *International Journal of Climatology* on the 2<sup>nd</sup> July 2024.

34 **Abstract**

35

36 Ignoring a correlation between flooding and extreme winds underestimates risk to insurers or providers of  
37 critical infrastructure such as railways or electricity. We explore this potential underestimation for Northwest  
38 Europe, illustrated using Great Britain (GB), using an event-based analysis in regional 12 km UK Climate  
39 Projections (UKCP18, 1981-1999, 2061-2079 – RCP8.5). We derive a new wintertime (Oct-Mar) set of 3,427  
40 wind events to match an existing set of fluvial flow extremes and design innovative multi-event *episodes* ( $\Delta t$  of  
41 1-180 days long) that reflect how periods of adverse weather are actually experienced (e.g. for damage).  
42 Results show the probability of co-occurring wind-flow episodes in GB is underestimated 2-4 times if events are  
43 assumed independent. Significantly, this underestimation is greater both as severity increases (e.g. 90<sup>th</sup> to 99<sup>th</sup>  
44 percentile) and  $\Delta t$  reduces, adding the insight that we need to be most concerned about underestimating co-  
45 occurrence in the strongest individual or closely consecutive storms ( $\Delta t \sim 3$ ). In the future, joint extremes are  
46 twice as likely as in the present. Statistical modelling demonstrates that changes go significantly beyond  
47 thermodynamic expectations (i.e. more high flows in a wetter climate). The largest co-occurrence increases are  
48 shown to be in mid-winter (DJF) and changes in the north Atlantic jet stream dynamics are demonstrated to be  
49 an important driver; particularly in mid-winter it is strengthened and squeezed into a southward-shifted  
50 latitude window (45-50°N), conditions typical of high flows and joint extremes impacting GB in present day  
51 simulations. More widely, that work highlights that the recipe of driving large-scale conditions (e.g. jet stream  
52 state) for a multi-impact ‘perfect storm’ will vary by country. So, future analyses should work to build area-by-  
53 area understanding of how the impact of common drivers varies spatially, which is key to risk mitigation and  
54 planning (e.g. diversification, mutual aid across Europe).

55

56

57

58 **Keywords:** Jet stream, multi-hazard, seasonality, squeezed, episodes, flooding, extreme wind

59

60 **1. Introduction**

61

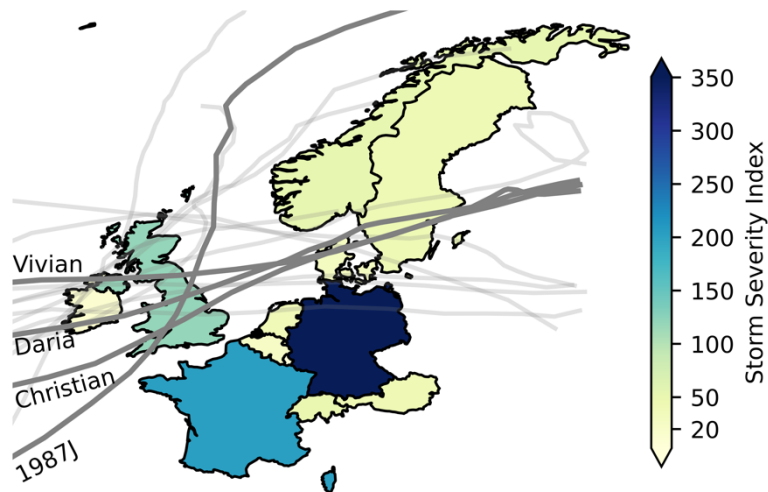
62 The challenge of multi-hazard risk has long been recognised for storms (e.g., Southern, 1979; White, 1974) and  
63 more broadly (Gallina et al., 2016; Hillier, 2017; Kappes et al., 2012; UNEP, 1992; Ward et al., 2022). This co-  
64 occurrence of adverse natural events has also recently been framed as ‘compound’ (e.g., Simpson et al., 2021;  
65 Zscheischler et al., 2018). In short the difficulty is that impacts occurring together, colloquially referred to as  
66 ‘perfect storm’, are harder to handle (Hillier et al., 2023) and impacts potentially combine to amplify beyond  
67 the sum of the constituent parts.

68

69 Inland flooding and extreme winds event cause the largest losses in North-West Europe (Mitchell-Wallace et  
70 al., 2017; PERILS, 2024). Illustratively, during 16<sup>th</sup>-21<sup>st</sup> February 2022 a sequence of storms named Dudley,  
71 Eunice and Franklin inflicted various hazards including flooding and extreme winds across the UK and  
72 Northwest Europe (Mühr et al., 2022; Volonté et al., 2023a, b), resulting in multi-sector impacts (e.g. road,  
73 power distribution) and nearly €4 billion in insured losses (Kendon, 2022; PERILS, 2023; Saville, 2022). Similarly,  
74 from 3<sup>rd</sup>-27<sup>th</sup> Dec 1999 the sequence Anatol, Lothar, Martin caused ~€10 billion insured property damage alone  
75 (PERILS, 2024; Roberts et al., 2014).

76  
77 Strikingly, most of the 98 impactful wintertime (Oct-March) wind or flood incidents in the PERILS database  
78 (PERILS, 2024) from 2010 to 2024 affect Great Britain (GB, 73), more than France or Germany (38 or 47,  
79 respectively). Moreover, wintertime correlation of proxies for flooding and wind in countries near GB appears  
80 similar (Bloomfield et al., 2023; Hillier and Dixon, 2020). This is likely because extra-tropical cyclones typically  
81 track eastwards from the Atlantic (e.g., Roberts et al., 2014) and are a key driver of both hazards across NW  
82 Europe (Fig. 1), which is illustrated by joint wind-flood events during named storms (e.g., Fink et al., 2009;  
83 Kendon and McCarthy, 2015; Liberato, 2014; Matthews et al., 2018). As such GB is a useful sentinel location for  
84 studying co-occurring flood-wind impacts in NW Europe.

85  
86  
87



88  
89 *Fig. 1: Indicative map of the distribution of severe wind in NW Europe from a sub-set of 25 storms that caused significant damage in the*  
90 *British Isles from two catalogues (PERILS, 2024; Roberts et al., 2014), for which ERA5 data are available (i.e. pre-2024). 16 pre-2021*  
91 *tracks are shown where data are available (light grey lines) (CCC, 2022) with 4 illustrative tracks labelled and named (dark grey lines).*  
92 *SSI is the Storm Severity index is  $v^3$  over 98<sup>th</sup> percentile (see Section 2.1) and is a total per country accumulated over the storms. Map*  
93 *projection: Plate carrée.*

94

95 Building on initial work establishing that a relationship existed (Hillier et al., 2015; Matthews et al., 2014), there  
96 is now strong evidence that floods and extreme wind co-occur in GB on daily to seasonal timescales  
97 (Bloomfield et al., 2023; De Luca et al., 2017; Hillier and Dixon, 2020; Jones et al., 2024; Martius et al., 2016;  
98 Owen et al., 2021b, a), perhaps controlled by the jet stream characteristics (Hillier and Dixon, 2020). Existing  
99 work predominantly uses heavy precipitation as a proxy for flooding (e.g., Vignotto et al., 2021). As reviewed  
100 in Bloomfield et al (2023) studies using river flow or impact data, which more directly relate to flooding, are  
101 much less common in GB (De Luca et al., 2017; Hillier et al., 2015, 2020) or elsewhere (Küpfer, 2024). Indeed,  
102 even globally only three studies assessing dependency use river flow and wind derived from the same  
103 underlying climate model, two in GB (Bloomfield et al., 2023, 2024) and one globally for tropical cyclones  
104 (Stalhandske et al., 2024). Thus, future change in joint wintertime flood-wind risk remains of interest.

105  
106 Most recently, two studies have used the UK Climate Projections (UKCP18) to advance understanding of the  
107 drivers of the wintertime co-occurrence of potential flooding and extreme wind in GB, present and future.  
108 Bloomfield et al (2024) used 30 pre-defined weather types in the regional UKCP18 simulations (12 km spatial  
109 resolution) and a GB hydrological model to assess the meteorological drivers of joint wind and high flow  
110 extremes. For 1-day windows, using population-weighted severity indices, they found cyclonic weather types  
111 typical, and also confirmed the positive phase of the North Atlantic Oscillation (NAO+) as an associated state  
112 (Hillier et al., 2020). At a seasonal timescale they also demonstrated a future increase in years that will be both  
113 wet and windy. Manning et al (2024) used the convection permitting UKCP18 local (spatial resolution of 2.2 km)  
114 to investigate the role of storm track position and jet stream on the co-occurrence of wind and rain extremes.  
115 For individual storm events in mid-winter (December-February) they ascribed future change in co-occurrence  
116 to predominantly thermodynamic causes (i.e. warmer and therefore wetter) supported by a southerly  
117 disposition of the jet stream. Both papers find a 4-fold increase in short-duration joint events (i.e.  $\leq 1$ -day)  
118 into the future.

119  
120 This work builds on and adds to these studies in a number of unique ways. Using high flows rather than  
121 precipitation, it quantifies the co-occurrence of events ( $E$ ) within multi-hazard *episodes* ( $\epsilon$ ) spanning daily to  
122 seasonal (i.e.  $\Delta t = 1$ -180 days long) from October to March in the UKCP18 regional data (1981-1999, 2061-  
123 2079). It uses high flows as they do not simply arise from precipitation in individual storms, so the causative  
124 storm(s) might differ in character as might context (e.g. soil saturation) and associated jet stream dynamics. It  
125 examines the role of the jet stream in more detail, primarily by investigating the role of seasonality (i.e. the  
126 time-distribution of events within the winter). To do this it employs an accessible index that is widely used to  
127 characterise the latitude and strength of the North Atlantic jet (Woolings et al., 2010), with the intention of  
128 facilitating future inter-comparison between climate models. Finally, to give real-world relevance, and for  
129 technical reasons related to how the severity indices are built for longer time windows (see Section 2.2), it

130 develops an approach (dwECA) using dynamically positioned time windows to reflect how these multi-event  
131 windy episodes with high river flows ( $\Delta t = 1-180$  days) are actually experienced.  
132  
133 To define distinct claims (re)insurers commonly use windows of 72 hours for storms ( $\Delta t = 3$  days) or 21 days for  
134 floods called 'hours clauses' (e.g., Mitchell-Wallace et al., 2017; PERILS, 2023), which insurers will position to  
135 encompass the maximum loss possible. More widely, an observer (e.g. an emergency response manager) might  
136 say "*It started with the storm on Tuesday, and ended after the last heavy rain on Sunday*". To study individual  
137 weather phenomena (e.g. distinct storm) a buffer such as  $\pm 24$ h might be used (e.g., Manning et al., 2024;  
138 Martius et al., 2016), but it is less clear how to proceed for an episode containing storms over a longer period  
139 (e.g. 14-days), and non-overlapping windows or block maxima (e.g., Bloomfield et al., 2023; Zscheischler et al.,  
140 2021) may chop a storm in half. The proposed dynamic time windows for episodes ( $\varepsilon$ ) uses the weather  
141 events ( $E$ ) themselves to define the evident start and end of the adverse conditions. As such, dwECA is  
142 intended to align with stakeholder definitions and experience, with insurers providing a motivation to focus on  
143 time windows ( $\Delta t$ ) of 3 and 21 days. The work has real-world relevance as even in insurance, where natural  
144 hazard risk modelling is quite mature (e.g., Mitchell-Wallace et al., 2017), because flooding and extreme wind  
145 models of NW Europe are still independently derived, namely based on uncorrelated underlying climate  
146 simulations (Dixon et al., 2017; Hillier et al., 2024).

147  
148 Using the idea of framing multi-hazard risk environments as an in-depth or user focussed case study to cut  
149 through complexity (Hillier and Van Meeteren, 2024; Ward et al., 2022) the work is framed by the insurance  
150 sector, yet results are more widely applicable. There are four main research questions:

- 151
- 152 1. Do the most severe extreme winds and flows tend to co-occur or not? Namely, are they asymptotically  
153 dependent?
  - 154 2. How does strength of co-occurrence vary with the time-window ( $\Delta t$ ) used to group events into  
155 episodes?
  - 156 3. Can a relatively simply derived metric of jet position be a functional, readily applied tool to distinguish  
157 jet states characteristic of co-occurrence?
  - 158 4. How do future changes in the North Atlantic jet stream influence co-occurrence in simulations of the  
159 future?

160

## 161 **2. Data & Methods**

162

163 The workflow in Fig. 2 is used to produce individual events for wind ( $E_W$ ) and flood ( $E_F$ ) with timestamps from  
164 the same underlying climate model (i.e. UKCP18). Then, from these, multi-hazard *episodes* ( $\varepsilon$ ) are created and

165 analysed. All metrics are calculated during extended winter (October–March) and nationally aggregated.  
 166 Threshold values are defined at percentiles derived from the present-day climate simulations, then are applied  
 167 to future climate to understand potential changes.

168  
 169 Existing data and practice (e.g. thresholds, definitions) are adopted to create events and define their severity  
 170 (Bloomfield et al., 2023; Griffin et al., 2022a, b; Manning et al., 2024). As such, detail is provided in Appendix A.  
 171 Importantly, the rank correlation between GB aggregated precipitation, high river flows and extreme wind for  
 172 the simulated present (1981-1999) in UKCP18 closely matches multiple historic weather datasets and river-  
 173 flows derived from them across time windows from 1 to 180 days (Bloomfield et al., 2023, 2024; Harrigan et  
 174 al., 2023; Hersbach et al., 2020; Hirpa et al., 2018). Indeed, these correlations have also been verified against  
 175 impacts on the GB rail network (Bloomfield et al., 2023). Thus, the UKCP18 simulations appear to adequately  
 176 capture the level of co-occurrence between extreme winds and high flows (detail in Appendix A.1).

### 177 178 2.1. Defining events ( $E$ ) for each separate hazard

179  
 180 Each event ( $E$ ) is a grid of the maxima of a hazard driver (e.g.  $v$ ) during a time-window containing an isolated  
 181 hydro-meteorological extreme (detail in Appendix A.2). For each event, summary metrics (total area, duration,  
 182 severity index) are assigned to a single date  $t_{max}$ , the individual day during the event when the greatest  
 183 number of grid cells exceeding the set threshold level. An event's Storm Severity Index,  $SSI(E)$  follows Klawa  
 184 and Ulrich (2003) as given by Eq. (1) and Table 1, detailed in Appendix A.3:

185  
 186 Eq. (1) 
$$SSI(E) = \sum_{i=1}^{N_i} \sum_{j=1}^{N_j} \left( \frac{v(E)_{ij}}{v_{i,j}^{98}} - 1 \right)^3 \cdot I_{i,j}$$

187 
$$I_{i,j} = \begin{cases} 0 & \text{if } v(E)_{i,j} < v_{i,j}^{98} \\ 1 & \text{otherwise} \end{cases}$$

188  
 189 *Table 1: Table of parameters used, with precipitation included for completeness (see Appendix A).*

Parameter	Symbol	Units
Maximum daily 10 m wind gusts at a grid cell $i,j$ , and the threshold (98 <sup>th</sup> ) percentile taken to define extreme at a grid cell.	$v_{i,j}, v^{98}$	$ms^{-1}$
Total daily precipitation, and the threshold (98 <sup>th</sup> ) percentile taken to define extreme at a grid cell.	$p, p^{98}$	$mm$
Daily mean river flow	$q$	$m^3s^{-1}$
Day	$t$	days
Event (e.g. event ID $k = 1247$ for wind). $W$ is for Wind, $F$ is for river flows and $P$ is precipitation.	$E_{W,k}$	-
Multi-hazard episode $\varepsilon$ , with its type (wind $W$ , high flow $F$ , joint $J$ ) and SI percentile exceeded	$\varepsilon_W^{95}$	-

for events within it (75 <sup>th</sup> , 95 <sup>th</sup> , 99 <sup>th</sup> ). Also see Fig. 3.		
Event's most extreme day, to which summary statistics (e.g. duration, FSI) are assigned.	$t_{max}$	days
Temporal limits of an event (i.e. start and end)	$t_{start}, t_{end}$	days
Length of multi-hazard episode, 'time window'	$\Delta t$	days

190

191

192 For, simplicity and to avoid a judgement linking value directly to population density (e.g. consider a wind farm),  
 193 no population weighting is used. The optimal formulation of SSI (e.g. power-law, exponential, wind threshold,  
 194 storm duration) is still actively debated. Most pertinently, probabilistic models that account for the uncertainty  
 195 in how individual assets are damaged (Heneka et al., 2006; Heneka and Ruck, 2008; Pardowitz et al., 2016;  
 196 Prah et al., 2012) better approximate losses in Germany across all 2004 wintertime days in 11 years (1997-  
 197 2007). The exception to this is the costliest days (~10 per year), which are still adequately modelled using cubic  
 198 excess-over-threshold approach with a 98<sup>th</sup> percentile (Prah et al., 2015). Thus, using Eq. (1) is appropriate  
 199 here. Because recent developments have not been previously reviewed, a detailed justification is in Appendix  
 200 A.3. The new wind event set is described in Appendix A.4.

201

202 Based on the form of SSI, Flood Severity Indices (FSI) have recently been developed (Bloomfield et al., 2023).  
 203 Only grid cells on the river network are used, again with no population weighting. Thus, each events' flood  
 204 severity  $FSI(E)$  is given by Eq. 2 and Table 1.

205

206 Eq. (2)

$$FSI(E) = \sum_{i=1}^{N_i} \sum_{j=1}^{N_j} \left( \frac{q(E)_{i,j}}{q_{i,j}^{99.5}} - 1 \right) \cdot I_{i,j}$$

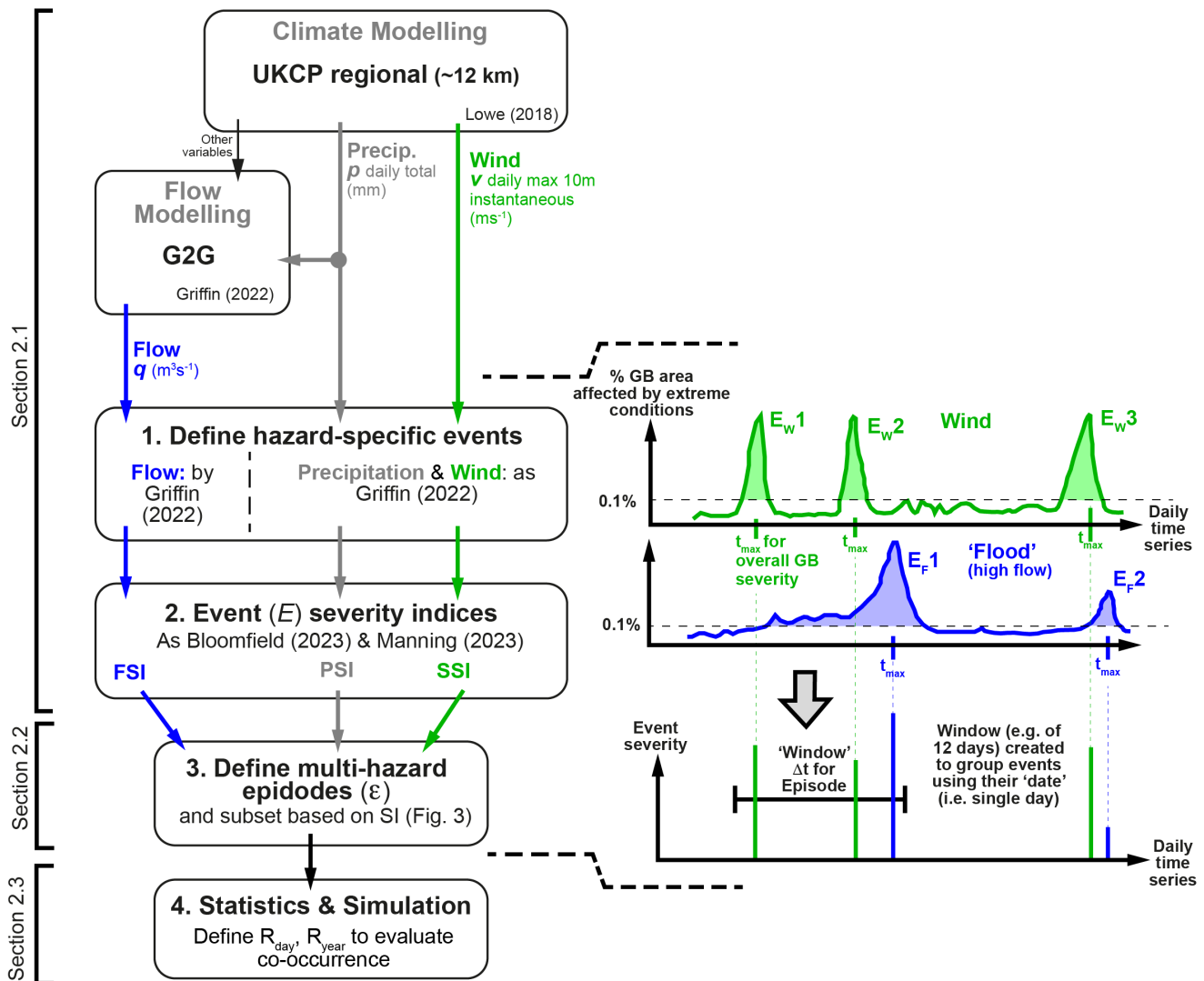
207

$$I_{i,j} = \begin{cases} 0 & \text{if } q(E)_{i,j} < q_{i,j}^{99.5} \\ 1 & \text{otherwise} \end{cases}$$

208

209 Debate on the form of FSI is expected to continue, so a detailed justification is in Appendix A.3. Pertinently, FSI  
 210 as configured in Eq. 2 is suitable here as only the most extreme events are selected (i.e. >75<sup>th</sup> percentile of  
 211 events). Furthermore, this is 5-6 high flows per year, comparable to the ~7 floods per year in commercial risk  
 212 models (Hillier et al., 2024).

213



214

215

216

217

218

219

220

221

## 222 2.2. Defining multi-hazard episodes ( $\epsilon$ )

223

224

225

226

227

228

229

Extratropical cyclones cluster in time, with 2 or 3 meteorologically distinct cyclonic systems (Mailier et al., 2006; Vitolo et al., 2009) combining in longer windy periods. Similarly, rainy days occurring in succession might be grouped in episodes (Kopp et al., 2021). Here, this concept is applied to multi-hazards (Fig. 2), adopting the term *episode* ( $\epsilon$ ) and applying it to mean a grouping in time of hazardous events ( $E$ ) within a selected spatial domain as is established practice when hazards co-occur (e.g., Bloomfield et al., 2023; De Luca et al., 2017; Hewitt and Burton, 1971; Hillier et al., 2015; Kappes et al., 2012). In this case the domain is set to GB. The

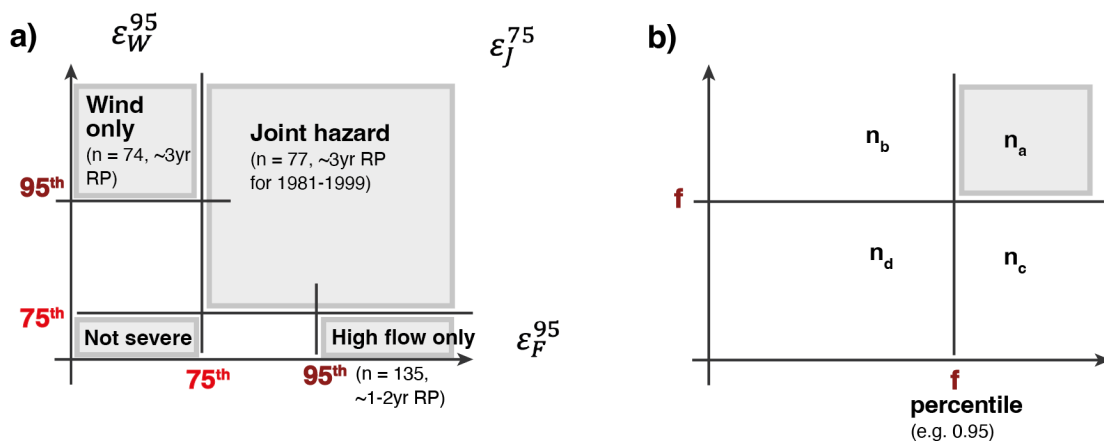
230 temporal grouping approach is related to the time-lag method promoted by Claassen et al. (2023) except that  
 231 the time-lag here might also be due to impact related factors (e.g. time to develop, repair or recovery time,  
 232 staff fatigue, an organisation’s reporting timeframe, an April-March financial year) not just duration and overlap  
 233 of physical hazard (e.g., Hillier et al., 2023; Hillier and Dixon, 2020; de Ruiter et al., 2019).

234  
 235 Episodes are defined by starting with the event with greatest severity index (SI), placing a window of length  $\Delta t$   
 236 days around it positioned to capture other events that create the largest total SI (see Fig. 2), and removing  
 237 these events. Then, this is repeated until all events are accounted for. Once created, episodes’ severity must be  
 238 quantified.

239  
 240 That flood-wind co-occurrence might be raised by a preponderance of an NAO+ state across a 180-day season  
 241 (Bloomfield et al., 2024; Hillier et al., 2020) raises the technical question of how to quantify severity for long  
 242 episodes. This depends on stakeholder and purpose. It is possible to simply sum daily SSI or FSI (Bloomfield et  
 243 al., 2023), implicitly assuming that each day is independent and additive in its impact (i.e. duration/persistence  
 244 is significant). Is being flooded at 2.0m depth for 5 days five times more damaging than for 1 day? For an  
 245 electricity network operator fined by customer minutes lost, it might be (Wilkinson et al., 2022). As the  
 246 strongest gusts or highest river levels during an event approximate insured damage well (Mitchell-Wallace et  
 247 al., 2017), an alternative is to use an event-based approach (e.g., Griffin et al., 2022b; Roberts et al., 2014),  
 248 then sum events’ losses. This implicitly assumes a reset between events, ignoring duration (Appendix A.3) and  
 249 is the (re)insurance approach followed in Fig. 4.

250  
 251 In this paper, however, the main purpose is to study co-occurrence of large events that drive risk. So, episodes  
 252 ( $\epsilon$ ) are classified by the severity of their constituent events (Table 1), with thresholds chosen to select  
 253 potentially impactful events (Section 2.1, Appendix A.3) and mutually exclusive subsets containing roughly  
 254 equal numbers of episodes (i.e. RPs) (Fig. 3). This classification is *not* a summation. Illustratively,  $\epsilon_W^{95}$  contains at  
 255 least one wind event  $E_W$  with an SSI in the top 5% of wind events but no high flow event.

256



257

258 Fig. 3: a) Illustration of subsets and nomenclature used, with numerical detail for  $\Delta t = 3$  in the present day from Fig. 4a.  $\varepsilon_j^{75}$  is the subset  
259 of all episodes with both hazards jointly having at least one event exceeding the 75<sup>th</sup> percentile. Also see Table 1. b) Nomenclature used  
260 to define  $U$  (Section 2.3).

### 261 2.3. Statistical simulation for co-occurrence analysis

262

263 A variety of options exist to quantify dependency of hydro-meteorological extremes (e.g., Bevacqua et al.,  
264 2021; Heffernan and Tawn, 2004; Serinaldi and Papalexiou, 2020), although it is advised to ensure that they  
265 are not reinvented or untested (Serinaldi et al., 2022). One well-established approach is using copulas to fit a  
266 distribution to data extreme in both variables (e.g., Bevacqua et al., 2017; Manning et al., 2024). This permits  
267 smoothed curves to be fitted, but relies upon selecting an appropriate distribution (e.g. Gumbel copula).  
268 Alternatively, extremal dependency for wet and windy conditions can be quantified by measures of the co-  
269 occurrence of extremes above a given percentile (Hillier et al., 2015; Martius et al., 2016; Owen et al., 2021a).  
270  $\chi$  (Coles et al., 1999) and uplift in co-occurrence  $U$  (De Luca et al., 2017; Hillier et al., 2015) are closely related  
271 (Eq. 3, 4) with nomenclature in Fig. 3b.

272

273 Eq.3 
$$\chi = \frac{n_a}{(1-f)n}$$

274

275 Eq. 4 
$$U = \frac{n_a}{E[n_a]} = \frac{n_a}{(1-f)^2 n}$$

276

277  $\chi$  is the probability that one variable is extreme if the other is also extreme, varying between 0 and 1 (e.g.,  
278 Bloomfield et al., 2023; Vignotto et al., 2021).  $U$  is an occurrence ratio, the observed number of co-  
279 occurrences divided by the number expected due to chance for independent events (i.e.  $E[n_a]$ ). It is also,  
280 therefore, the extent to which one would underestimate the probability of co-occurrence if independence  
281 were assumed. Some authors have called  $U$  a ‘Likelihood multiplication factor’ (Ridder et al., 2020; Zscheischler  
282 and Seneviratne, 2017). With independent events uniformly distributed over a time period, the significance of  
283  $U$  is found with a binomial test (Bevacqua et al., 2021), but  $E[n_a]$  can also be simulated directly.

284

285 Event Coincidence Analysis (ECA) is a method in time-series analysis to assess if one type of event might be a  
286 precursor to another based on an underlying Poisson process (e.g. netCoin or CoinCalc R packages) (Donges et  
287 al., 2016; Escobar, 2015; Siegmund et al., 2017). It is unclear to us, with the dynamic positioning of the  
288 window and 1 to  $n$  events potentially within each episode, how to construct this analytically. So, statistical  
289 simulation modelling (e.g., Hillier et al., 2015; Ridder et al., 2020) is used to investigate  $U$  in UKCP18 by  
290 eliminating elements of its temporal structure (Hillier et al., 2015, 2020; Hillier and Dixon, 2020; Zscheischler et  
291 al., 2021). In this ECA using dynamic windows (dwECA), two simpler (i.e. less structured) models of events are  
292 created, from which episodes are then formed in Section 2.2.

293

- 294 1.  $R_{\text{day}}$ : For each event, year and day are randomised, a uniform distribution. This is  $E[n_a]$ , reflecting an  
295 Oct-Mar climatology approach (e.g., Champion et al., 2015; Smith and Phillips, 2012; Stephan et al.,  
296 2018), or a business-as-usual case in (re)insurance (e.g., Hadzilicos et al., 2021; Hillier et al., 2024).
- 297 2.  $R_{\text{year}}$ : For each event, only year is randomised. All relationships to proximal events within a time-series  
298 are broken up to and including inter-seasonal timescales, yet seasonality (i.e. the pattern of frequency  
299 as time progresses through a winter) is retained. This avoids pre-supposing a Dec-Feb peak storm  
300 season (e.g., Manning et al., 2024; Martius et al., 2016), as this may change in future.

301

302 Note that all randomisation is conducted separately within each ensemble member. This is cautious (i.e.  
303 perhaps less significant  $p$ -values) but remains valid even if the 12 ensemble members of UKCP18 are not a truly  
304 random sample. Randomisation is repeated 5 times, giving 1140 simulated years in total, 228 for each  
305 statistical model run. The chance ( $p$ -value) of occurrences in UKCP18 occurring in the simplified models can  
306 then be assessed by taking each as a null hypothesis  $H_0$  (i.e. Fig. 5, Fig. 6). Here, for episodes, uplift  $U_\varepsilon$  is the  
307 total count of the number events ( $n_a$ ) over threshold within episodes.

308

#### 309 2.4. Jet Stream metrics

310

311 One widely used and relatively simple metric of jet position is that of Woolings et al. (2010). This diagnostic  
312 uses four low-level wind fields (925-700 hPa) to quantify the latitude and speed of the eddy-driven jet stream.  
313 It is zonally averaged over the North Atlantic (0-60°W, 15-75°N), low pass filtered with a 10-day window to  
314 remove effects from individual synoptic systems, then the maximum westerly wind speed across the latitudes  
315 is taken to locate and quantify the jet. Data used here (McSweeney and Bett, 2020) are taken from the UKCP18  
316 global model, which drives the regional model used in this paper.

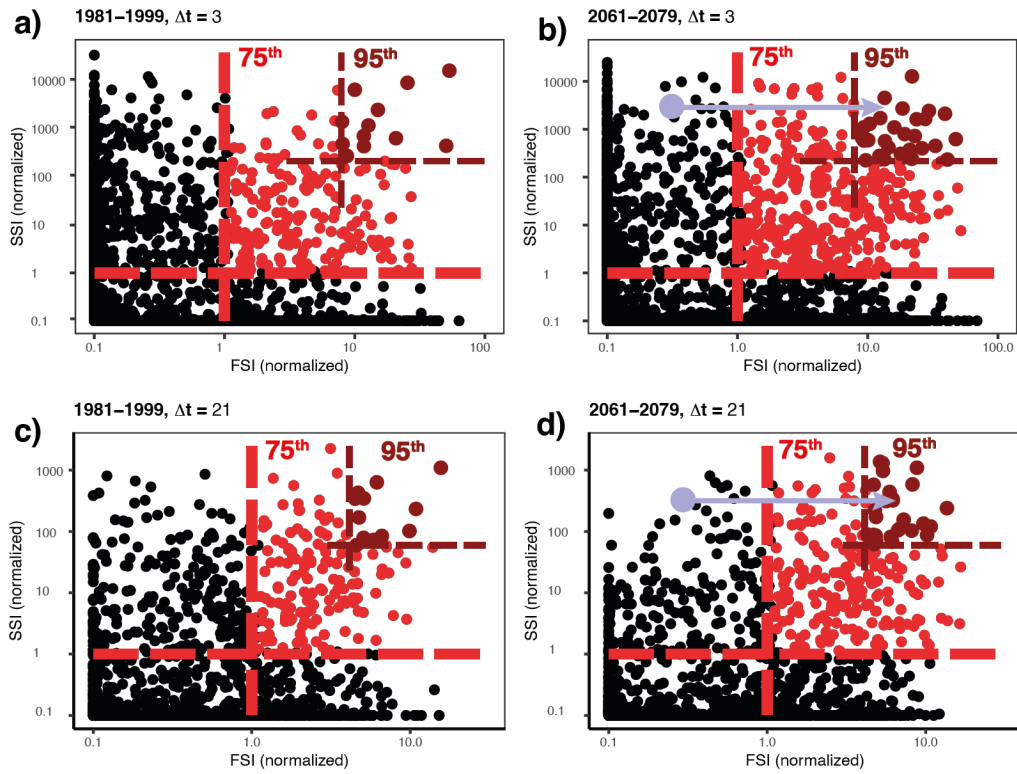
317

### 318 3. Results

319

320 Visually, on Fig. 4, a first impression is that the number of more severe joint episodes ( $\varepsilon_j$ ) increases in a future  
321 climate. This is investigated further for a range of time periods and thresholds (Section 3.1). Then, distribution  
322 by month or 'seasonality' is explored (Section 3.2). Finally, the jet stream is examined as a possible cause of the  
323 observed patterns (Section 3.3).

324



325

326

327

328

329

Fig. 4 Scatter plots of the summed severity of potential flooding (FSI) and extreme wind (SSI) for 3-day episodes for a) present and b) future time slices relative to the 75<sup>th</sup> percentile of these measures. Two thresholds are shown, the 75<sup>th</sup> percentile (red) and 95<sup>th</sup> percentile (dark red). Thresholds for 1981-1999 are used in all panels. d) and e) are the same, but for 21-day episodes. Light blue arrows visually highlight the tendency for FSI to increase into the future, which is particularly prominent for  $\Delta t = 21$ .

330

### 3.1. Uplift factors

332

333

334

335

336

Uplift ( $U_\varepsilon$ ) is the number of times is more common co-occurrences are in UKCP18 than expected for independent events uniformly distributed across Oct-Mar (i.e.  $R_{\text{day}}$ , pink). Fig. 5a clearly shows two patterns (red lines) for the present.

337

338

339

340

341

1.  $U_\varepsilon$  is broadly two to four for all  $\Delta t$  (1-180 days) and percentiles (75<sup>th</sup> to 99<sup>th</sup>), but difficult to detect for seasonal timescales.
2.  $U_\varepsilon$  is highest for more extreme events (i.e. rarer, larger percentiles) and at shorter time windows (i.e. smaller  $\Delta t$ ).

342

343

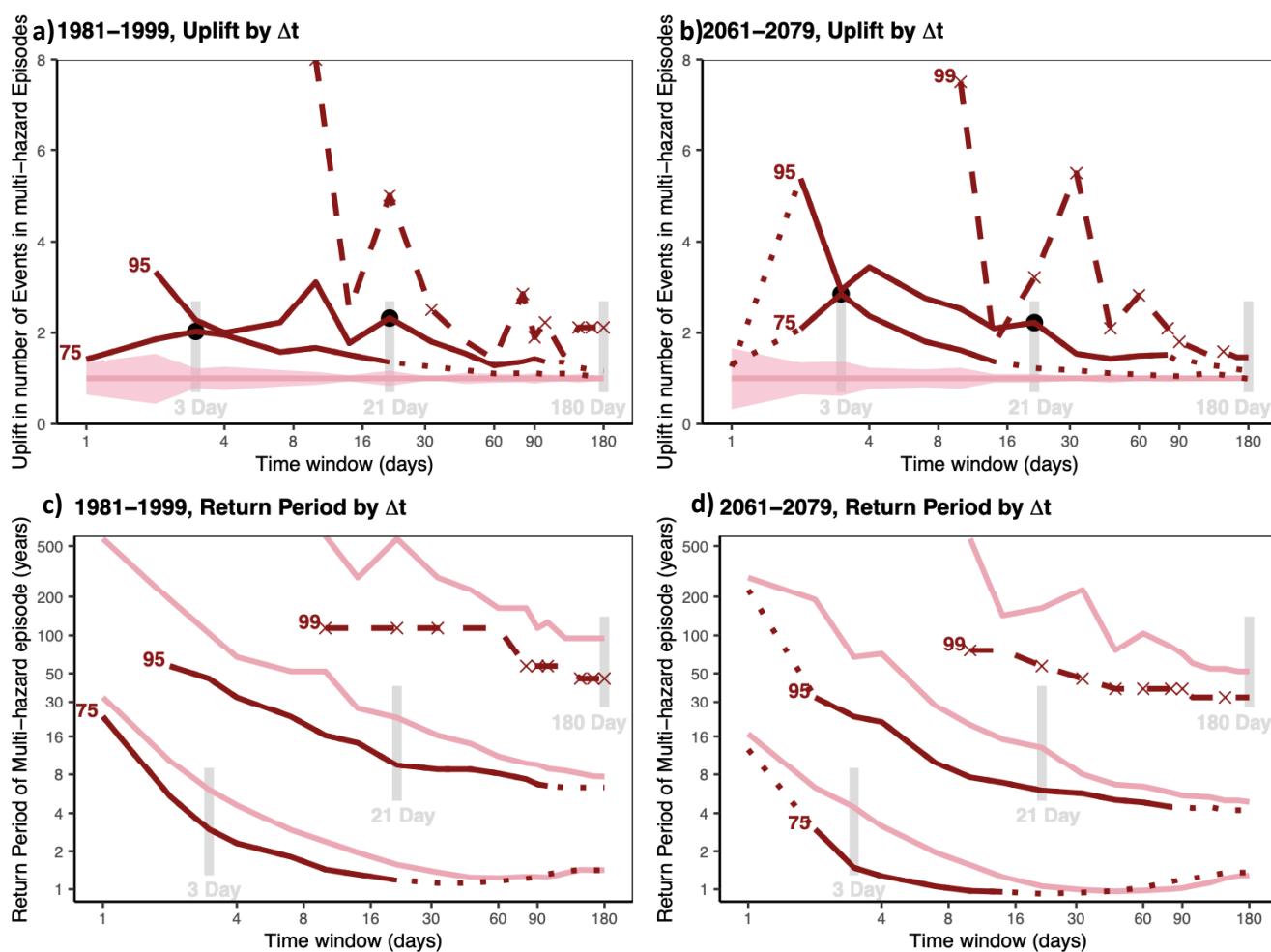
344

345

346

Visually,  $U_\varepsilon$  is similar in future (Fig. 5b), best seen by comparison to the grey vertical lines which are identical in each panel. As  $U_\varepsilon$  is relative to a baseline ( $R_{\text{day}}, E[n_a]$ ) that accounts for the total of severe events ( $n_a + n_b + n_c$ ) increasing in future, it isolates the potential change in the dependence structure (i.e. level of ‘correlation’). Illustratively, for  $\Delta t = 3$  at the 95<sup>th</sup> percentile in 2061-2079 ( $\varepsilon_j^{95}$ ), a 104-year return period assuming independence is actually 23 years when accounting for dependence. Return periods (RPs) in Fig. 5c,d are

347 simply calculated for *episodes* (i.e.  $RP = \text{years}/n_\epsilon$ ), and so reflect the increased number of high-flow events in  
 348 RPs reduced to about half their present value.  
 349  
 350 For 1-day windows, the act of collapsing events to a single day ( $t_{max}$ ) will tend to underestimate co-  
 351 occurrence, as flooding is expected to peak the day after wind given that water takes time (typically up to 24h)  
 352 to flow into and through GB's rivers (De Luca et al., 2017); daily or storm-based analyses (Bloomfield et al.,  
 353 2023; Manning et al., 2024) will be less influenced in this particular.  
 354  
 355



356  
 357  
 358 *Fig. 5: Enhancement in co-occurrence, for a range of window lengths ( $\Delta t$ ) used to create episodes. a) Uplift in number of events involved*  
 359 *in multi-hazard episodes (1981-1999) as compared to a baseline of independence (pink line,  $R_{day}$ ). Solid red lines are statistically*  
 360 *significant, unlikely from variability within the independent case (pink shading is  $2\sigma$ ) assessed by simulation. Joint episodes  $\epsilon_j^{75}$  are*  
 361 *labelled '75', and so on. The Black dots situate the analyses of Fig. 6 within this plot. Dashed line indicates lower subjective confidence*  
 362 *as occurrences get low, with x marking statistically significant points. Dotted lines on Fig. 5 indicate that caution is needed, where*  
 363 *episodes occupy >10% of time because 'remnant' time periods left between already created episodes might start to appear, or where the*  
 364 *observation is not clearly different from the baseline (i.e.  $p > 0.05$ ) because  $n$  becomes low or the difference small. c) & d) Return period*  
 365 *of multi-hazard episodes at 3 percentiles (75, 95, 99). Note that the grey bars are identically positioned on a) and b), and on c) and d).*

366

### 367 3.2. Seasonality

368

369 Distribution by month of the co-occurrence of severe episodes, their seasonality, is explored in Fig. 6 at the key  
370 timescales of  $\Delta t = 3$  and 21 days using  $\varepsilon_j^{75}$  and  $\varepsilon_j^{95}$ , respectively. Since a longer window is more likely to contain  
371 extreme events, a higher threshold captures sufficient events for  $\Delta t = 21$ . There are three pertinent features:

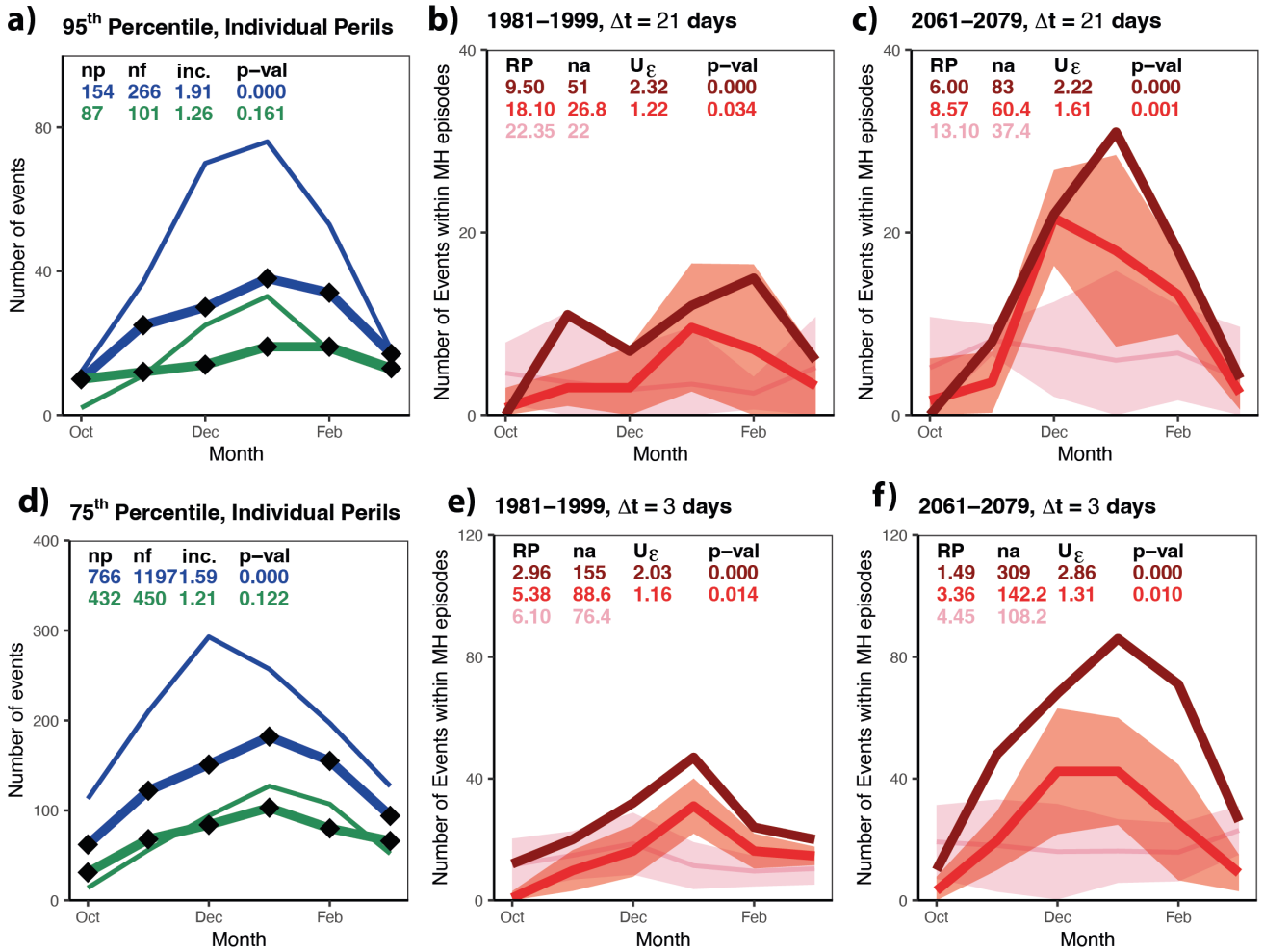
372

- 373 1. Considered individually (Fig. 6 a,d), both high flows and wind are notably more seasonal in future,  
374 more concentrated in December and January. This effect is greater for the higher (95<sup>th</sup>) percentile.
- 375 2.  $U_\varepsilon$  is 2-3, present and future, aligning with Fig. 5.
- 376 3. For  $\Delta t = 21$ , the red line ( $R_{\text{year}}$ ) is only a little below the UKCP18 occurrences (dark red), so at a storm-  
377 sequence timescale of weeks ( $\Delta t = 21$ ),  $U$  can largely be modelled by seasonality (i.e.  $R_{\text{year}}$ ). However,  
378 on a shorter timescale ( $\Delta t = 3$ ), an additional physical mechanism must be invoked that operates on a  
379 shorter time-scale, that of a single storm or storms in fairly rapid sequence (i.e.  $\Delta t \sim 2\text{-}10$  days).

380

381 Note that the seasonality effect in this bootstrap modelling ( $R_{\text{year}}$ , Fig. 6c) arises simply due to more events  
382 being placed (e.g. by a broader-scale atmospheric driver) in a restricted timeframe. Illustratively, consider a  
383 daily analysis 10 winters of 100 days, containing 50 floods and 50 wind extremes in total. If uniformly  
384 distributed (i.e. Poisson randomness), the expected number of co-occurrences is  $0.05 \times 0.05 \times 1000 = 2.5$   
385 coincidences (e.g., Bevacqua et al., 2021; Hillier et al., 2015). Now, compress these into the central 50 days, the  
386 expectation is  $0.1 \times 0.1 \times 500 = 5.0$  coincidences.

387



388

389

390

391

392

393

394

395

396

397

398

399

400

401

402

403

404

405

Fig. 6: Seasonality of individual events ( $E$ ) and multi-hazard episodes ( $\epsilon$ ). a) Seasonality of events for all high-flows (blue) and extreme wind (green) exceeding the 95<sup>th</sup> percentile. Thick lines are present day (1981–1999) and thin lines are the future (2061–2079).  $n_p$  &  $n_f$  are counts for the present and future, respectively. ‘inc.’ is the mean increase (multiplier) from present to future for the 12 ensemble members with the  $p$ -value is assessed using their variability (t-test). b) and c) Number of events in multi-hazard episodes  $\epsilon_j^{95}$  from UKCP18 (dark red), simulations with dependency broken but retaining seasonality (red,  $R_{year}$  model), and independent phenomena (pink,  $R_{day}$  model). Coloured ribbons are  $2\sigma$ , assessed by simulation. RP is return period of episodes in years, and  $p$ -values are calculated using variability of statistical model runs  $R_{day}$  and  $R_{year}$  (t-test). c) as for b) except for the future climate period. d-f) as for a-c), but for the 75<sup>th</sup> percentile and  $\Delta t = 3$ .

### 3.3. Jet Stream

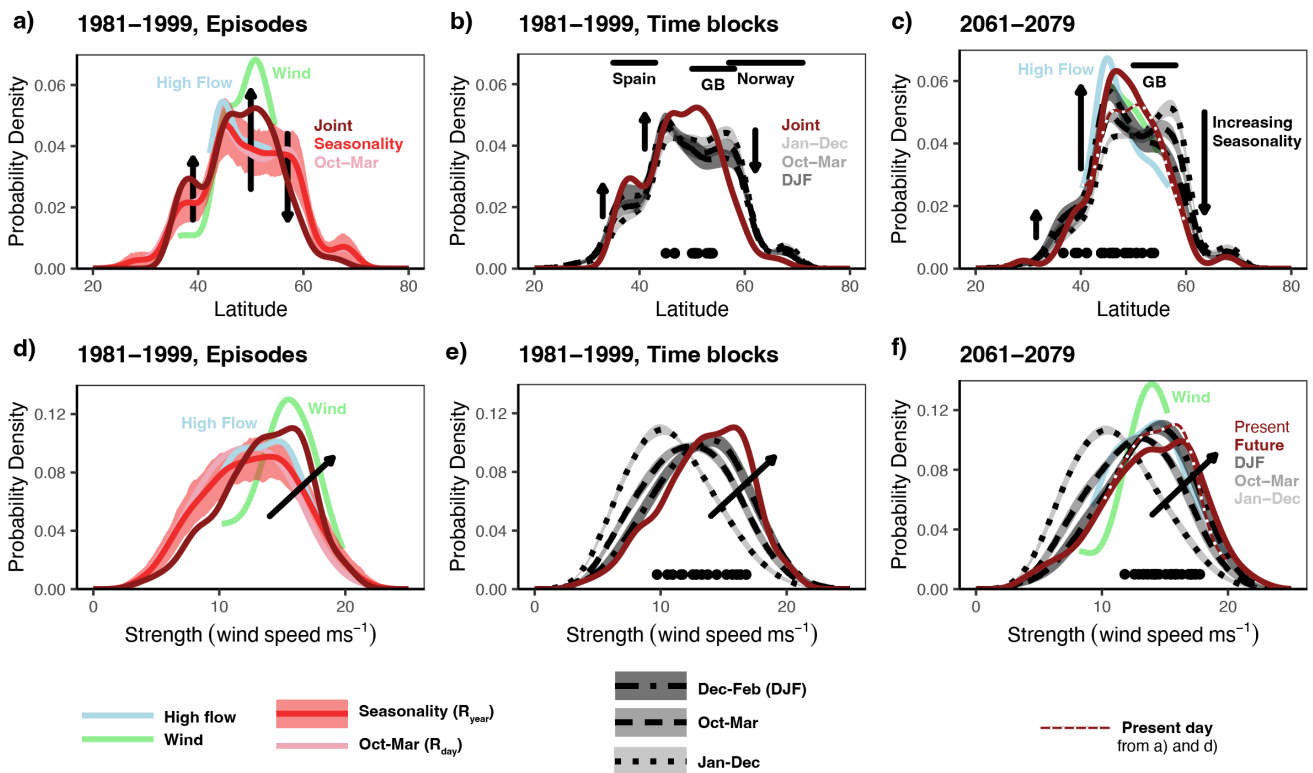
Fig. 7 investigates the jet stream as a potential physical mechanism for the uplift  $U$  that cannot be explained by seasonality for 3-day episodes ( $\epsilon_j^{75}$ ) identified in Section 3.2. Jet characteristics for the days of these episodes are plotted, with other subsets ( $\epsilon_F^{95}$ ,  $\epsilon_W^{95}$ ) (see Fig. 3a) and average values for time blocks (e.g. Dec-Feb) displayed for comparison. Fig. 8 presents a differently derived view, maps of westerly wind velocity anomalies on  $t_{max}$  days. Exact consistency between the two is not expected.

406

407 A number of features support the reliability and relevance of the main results to follow. First, in Fig. 7 subsets  
 408 (e.g.  $\varepsilon_j^{75}$ ,  $\varepsilon_W^{95}$ ) are distinct from time blocks and the statistical models ( $R_{\text{year}}$ ,  $R_{\text{day}}$ ). This simply would not happen  
 409 if there were a mis-match (e.g. in timing) between the metrics of the jet in the global model (McSweeney and  
 410 Bett, 2020) and extreme weather extracted here from the regional model. Second, the present day trimodal  
 411 peak in ERA-40/ERA-Interim, matched ‘reasonably well’ by UKCP18 (McSweeney and Bett, 2020; Woolings et  
 412 al., 2010), is present (Fig. 7a,b). Third, on days that severe weather occurs in GB jet-related wind anomalies  
 413 occur over NW Europe, not elsewhere, (Fig. 8) indicating that the jet metrics (McSweeney and Bett, 2020;  
 414 Woolings et al., 2010) are relevant to the study area.

415

416



417

418

419 *Fig. 7: Jet latitude (top row) and strength (bottom row) in UKCP18 (McSweeney and Bett, 2020) associated with  $\Delta t = 3$  joint high*  
 420 *flow and extreme wind episodes ( $\varepsilon_j^{75}$ ), present and future. Curves are density estimates (Gaussian kernel,  $\sigma = 1.0$  for strength and  $\sigma$*   
 421  *$= 2.0$  for latitude), and arrows illustrate trends identified in the data. In panels a) and d), the light red line is sampling preserving*  
 422 *the distribution of storms’ dates within a season (i.e.  $R_{\text{year}}$ ) and the pink lines are for Oct-Mar (i.e.  $R_{\text{day}}$ ) and the error ribbon is 10<sup>th</sup>-*  
 423 *90<sup>th</sup> quantiles for these storms as estimated from 100 random realisations. Uncertainty for the selected seasons (b,c,ef) is shown as*  
 424 *grey shading and is  $\pm 2\sigma$  stderr of the 12 ensembles of UKCP18. For visual clarity, only the parts of the wind and high-flow curves*  
 425 *( $\varepsilon_W^{95}$ ,  $\varepsilon_F^{95}$ ) are shown where they differ notably from the other curves. Dots are the most extreme events ( $\varepsilon_j^{95}$ ). Bars in b) and d)*  
 426 *show the latitude ranges of illustrative countries. All days within each episode are used.*

427 For 1981-1999 joint severe episodes' ( $\varepsilon_J^{75}$ , dark red line) jet strength and latitude differ discernibly from  
428 conditions at the times of year that they typically occur (i.e.  $R_{\text{day}}$ , red line and shading in Fig. 7) and from  
429 average Oct-Mar conditions ( $R_{\text{day}}$ ); Oct-Mar curves match those for non-severe storms ( $\varepsilon_J^{<75}$ ) very closely,  
430 although these are not shown for visual clarity (Fig. 7). Extremes also differ from a jet typical of the mid-winter  
431 DJF storm season. Specifically, the four differences are:

432

- 433 1. Days with only high flows ( $\varepsilon_F^{95}$ ) have jet latitude frequency peaks at 45°N, marginally elevated above  
434 the seasonal expectation (Fig. 7a). Similar is true for jet strengths (Fig. 7d, Fig. 8b).
- 435 2. Potentially damaging winds in isolation ( $\varepsilon_W^{95}$ ) are associated with a strong jet typically focussed on 45-  
436 55° latitude range (Fig. 7a,d) with a jet speed anomaly at relatively high latitudes (50-60°N) extending  
437 across the Atlantic (Fig. 8a).
- 438 3. Jet latitude for joint  $\varepsilon_J^{75}$  episodes peaks distinctly at 50°N (Fig. 7a,d, Fig. 8c). Self-evidently this is largely  
439 due to GB's latitude (Fig. 7b) because storms used here must impact GB, and the southwards  
440 displacement in this subset is highlighted with vertical arrows (Fig. 7a).
- 441 4. The peak in  $\varepsilon_J^{75}$  jet latitude is between the  $\varepsilon_F^{95}$  and  $\varepsilon_W^{95}$  peaks (Fig. 7a), and their jet strength is  
442 intermediate in a progression from the high-flow to wind curves (Fig. 7d, arrow). In map view, the joint  
443  $\varepsilon_J^{75}$  anomaly is also a blend of those from the individual hazards (Fig. 8a-c). A southerly lobe extending  
444 into the mid-Atlantic (20-40°W) is also notable.

445

446 Overall, co-occurring events in 1981-1999 appear to be associated with a jet that blends characteristics of the  
447 most severe high-flow inducing events (i.e. similar to expectations for the time of year) with the severest wind  
448 events. This is true even for the most severe episodes (i.e.  $\varepsilon_J^{95}$  shown as black dots,  $n = 5$  with a RP of 44.8  
449 years).

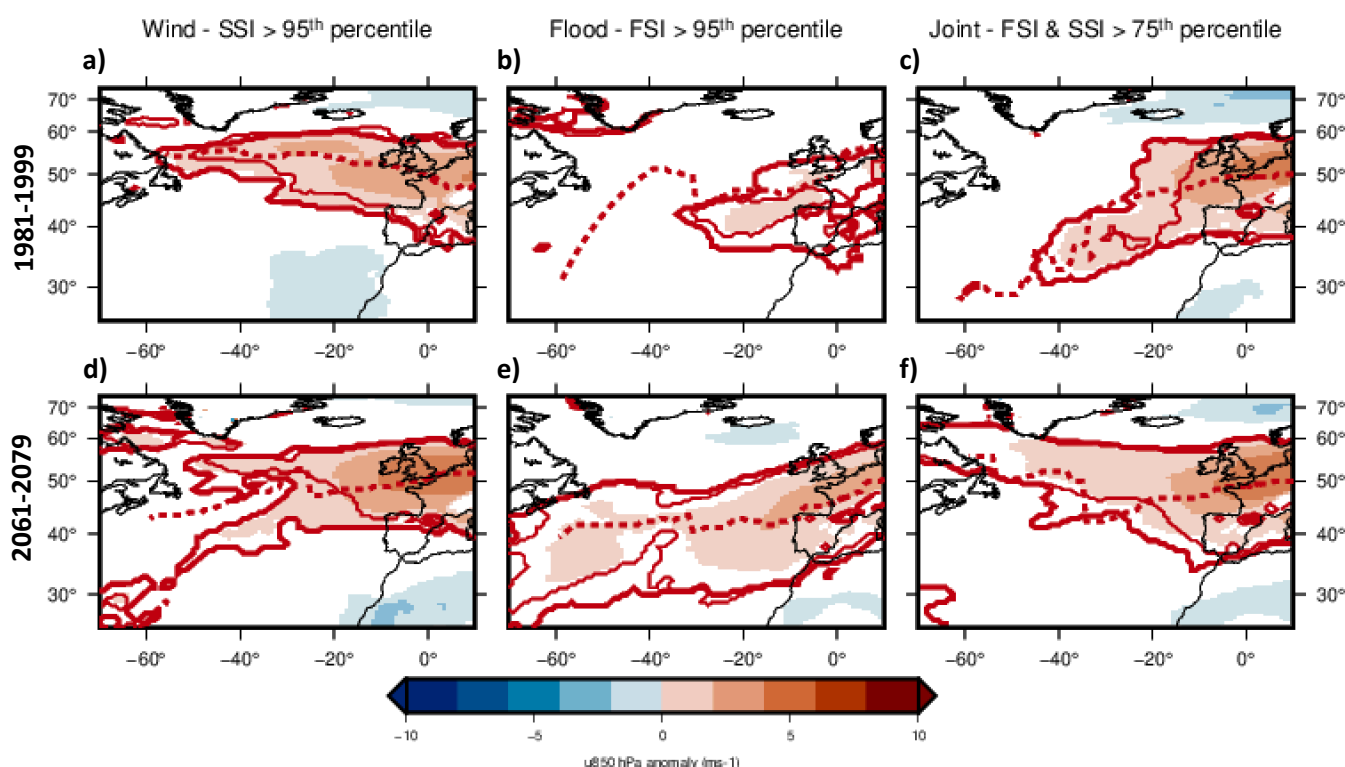
450

451 How does it change for 2061-79? Broadly, most patterns are similar in their character to 1981-1999, but with  
452 some important changes in relative magnitudes. The main changes are:

453

- 454 1. In future, jet strength and latitude anomalies ( $\varepsilon_J^{75}$ ,  $\varepsilon_W^{95}$ ,  $\varepsilon_F^{95}$ ) are of higher amplitude with respect to the  
455 1981-1999 levels (Fig. 7, Fig. 8), insensitive to the exact baseline chosen (e.g.  $R_{\text{year}}$ , non-severe).
- 456 2. For jet latitude, the peak for joint extremes ( $\varepsilon_J^{75}$ ) shifts  $\sim 3^\circ$  southwards, as do the conditions for the  
457 individual hazards, perhaps caused by the enhanced future seasonality of the jet which shifts  
458 southwards in midwinter despite an overall (Jan-Dec) shift northwards (Fig. 7c).
- 459 3. DJF jet strength in future becomes very similar to the present-day jet states for joint storms (Fig. 7f).
- 460 4. In map view (Fig. 8) anomalies for future wind episodes remain in a similar location, those for high  
461 flows expand south and west, and the anomaly for joint hazards like in 1981-1999 shares

462 characteristics with both; in Europe it extends to Iberia like for high-flows, but across the Atlantic at 50-  
 463 60°N like wind. This is a switch from a high-flow like pattern to a wind-like one (see Section 4.4).  
 464  
 465 In short, mean future DJF jet conditions tend to adopt a latitude that characterises high-flows in GB today and a  
 466 jet strength typical of joint extremes today (Fig. 7c,f). Thus, in future, typical shorter-term ( $\Delta t \lesssim 10$  days)  
 467 midwinter jet states appear like those characteristic of impactful compound storms today, aligning with the  
 468 observation that  $\varepsilon_j^{75}$  become more focussed in DJF (Fig. 6). The most severe episodes ( $\varepsilon_j^{95}$ ) reflect this, being  
 469 twice as frequent with a somewhat stronger and more southerly jet (i.e.  $n = 10$ , RP 22.4 years, Fig. 7).  
 470



471  
 472 *Fig. 8: Plan view of eddy-driven jet anomalies during stormy episodes ( $\Delta t = 3$ ) in comparison to the Oct-Mar climatology. Composites of*  
 473 *zonal wind velocity at 850 hPa for (a) dates of wind extremes ( $\varepsilon_W^{95}$ ,  $n=74$ ), (b) high-flow extremes ( $\varepsilon_F^{95}$ ,  $n=135$ ), and (c) days where both*  
 474 *are extreme ( $\varepsilon_j^{75}$ ,  $n=77$ ). (a)-(c) are for the present day i.e. 1981-2000, and (d)-(f) are for a future climate. Days used are only the most*  
 475 *severe day within an episode (i.e.  $t_{max}$ ). Solid red lines outline areas where the positive anomaly is significant ( $p < 0.05$ ) for one-tailed t-*  
 476 *t-test for difference between means of 12 ensemble members (climatology) and severe episodes. For comparison, thin red outlines are for*  
 477 *a DJF climatology, and dashed line is the most significant point at each longitude for a higher-level jet ( $u_{250}$ ). Hobo-Dyer (i.e. 37.5°*  
 478 *standard parallel) cylindrical equal area projection, with -30° meridian. Note that f) is reconciled with Fig. 7c by realising that those data*  
 479 *(u maximum) typically occur near NW Europe.*

480  
 481

#### 482 4. Discussion

483

484 Co-occurring flooding and extreme wind in GB are part of a complex multi-hazard risk (e.g., Simpson et al.,  
485 2021), and this paper considers these hazards using impact-based proxies (Hillier and Dixon, 2020), the  
486 UKCP18 dataset and modelled river flows (Griffin et al., 2022b). Its aim is to understand the joint hazard and its  
487 drivers. Other complexities, such as interactions between vulnerabilities or exposed infrastructure systems, are  
488 not considered. It offers:

489

- 490 1. A first examination of the jet stream for events based on high-flow conditions, not extreme rainfall, in a  
491 sentinel location for NW Europe
- 492 2. A multi-temporal ( $\Delta t = 1-180$  days) approach that groups events into multi-hazard *episodes* in a way  
493 that is relevant to stakeholders.
- 494 3. A new set of 3,427 wind events.
- 495 4. An examination of the role of seasonality in how high flows and extreme wind co-occur.
- 496 5. An assessment of relatively simple jet stream metrics (Woolings et al., 2010) in this context.

497

498 The work fits into a growing consensus on various aspects of potential episodes of joint wintertime flooding  
499 and extreme wind in GB. These episodes are typically driven by extra-tropical cyclones (e.g., Hillier et al., 2015;  
500 Manning et al., 2024; Owen et al., 2021a; PERILS, 2024), and associated with cyclonic or north-westerly  
501 weather patterns in an NAO+ regime (Bloomfield et al., 2024; Hillier et al., 2020). Fig. 5 reinforces an doubling  
502 in frequency in future climate projections, and also a x2-4 uplift ( $U$ ) in co-occurrence over a baseline of  
503 independence, a dependency that is not discernibly greater in future (Bloomfield et al., 2023; Manning et al.,  
504 2024). The jet stream associated with high river flows is to the south of GB, whilst for wind extremes it is to the  
505 north (Fig. 7a), consistent with ETCs being rainy on their northern flank and windy to the south (Manning et al.,  
506 2024). And, Fig. 7c shows that potential flooding tends to shift southwards in future (Bloomfield et al., 2024). It  
507 is also entirely in line with evidence that GB in future will be wetter (e.g., Lane and Kay, 2021; Lowe et al., 2019)  
508 with more frequent and severe high-flows (Collet et al., 2018; Griffin et al., 2022b). Despite being heavily  
509 validated, a caveat is that these studies rely on UKCP18, highlighting the need for a multi-model study. An  
510 important aspect of the agreement across varied approaches is that it demonstrates, through the episode  
511 definition used here, that previous work is applicable to (re)insurance and other stakeholders and their  
512 experience of episodes.

513

514 On this theme, what is an appropriate baseline? Namely, what statistical model (e.g. days of non-severe  
515 storms, uniform occurrence in DJF) should be chosen to represent independence between hazards for a  
516 particular enquiry? An insurer's standard practice might involve independence across an Oct-Mar season today.  
517 Then, illustratively (at  $\Delta t = 21$ )  $\varepsilon_F^{95}$  has a 1-year RP and  $\varepsilon_W^{95}$  has a 1-year RP, combining to be a 22-year RP joint  
518 episode assuming the  $R_{\text{day}}$  model, which is reduced 4-fold to a 6 year RP in 2061-2079 accounting for

519 dependence (Fig. 6b,c). If an insurer's modelling correctly includes the individual hazards seasonality, the  
520 correction needed would be notably less (Fig. 6). Thus, a fixed timeframe for analysis such as DJF or Oct-Mar  
521 (e.g., Zscheischler et al., 2021) should be used with caution, especially since peak months of (co-)occurrence  
522 may shift in future, and practitioners and researchers must ensure the statistical approach aligns with the  
523 research question posed.

524  
525 Selected aspects of the results are now discussed.

#### 526 527 *4.1. Co-occurrence for the most extreme events*

528  
529 The initial estimate of uplift in co-occurrence between extreme winds and high-flow in rivers was  $\sim 1.5$  times  
530 (Hillier et al., 2015). A value of  $\sim 2-4$  times in UKCP18 for daily data (Bloomfield et al., 2023) is now confirmed  
531 visually (Fig. 4) and statistically (Fig. 5, Fig. 6) for episodes like to cause loss (Appendix A.4), and appears robust  
532 in that it is not overly dependent on the method, metrics, or time period (1981-1999, or 2061-2079) used in  
533 the studies. Less well constrained is whether, in the limit, are these perils are asymptotically dependent or  
534 independent? Namely, do the most severe events have a weaker or stronger tendency to co-occur? This is a  
535 key question in assessing risk.

536  
537 For ERA5 wind gusts and precipitation or GLOFAS derived river flow (at daily, weekly, monthly resolution),  
538 residual tail dependence ( $\bar{\chi}$ )(Coles et al., 1999) does not tend to 1.0 as required for asymptotic dependence,  
539 but equally gives no indication that correlation disappears into the tail of the distribution, with the same true  
540 for monthly Network Rail delay data (Bloomfield et al., 2023; Vignotto et al., 2021). Indeed, in UKCP18 uplift  $U$   
541 increases from 2.4 to 3.4 as Bloomfield's threshold increases, an effect previously demonstrated by sensitivity  
542 testing (Hillier and Dixon, 2020). Fig. 5 extends this, with systematic increases in  $U$  from the 75<sup>th</sup> to 99<sup>th</sup>  
543 percentile ( $\varepsilon_j^{75}$  to  $\varepsilon_j^{99}$ ) indicating that more extreme episodes co-occur more strongly (Fig. 5a,b), at least to  
544 return periods of up to  $\sim 50-100$  years (Fig. 5c,d).

545  
546 Other metrics give a different view. Even as  $\bar{\chi}$  or  $U$  increase or hold steady with increasing threshold,  $\chi$  and  
547 Spearman's  $r$  decrease (Bloomfield et al., 2023; Hillier and Dixon, 2020). Taking this further, for rain and wind,  
548 with a Clayton copula best fitting their severity metrics for (UKCP18, 2.2 km) Manning et al (2024) implicitly  
549 assume asymptotic independence for the most extreme events. Indeed, by taking parts of two winter seasons  
550 and summer (i.e. Jan-Dec) it is possible to find negative correlations at higher thresholds and annual  
551 timeframes (Jones et al., 2024). The variety highlights the importance of using measures attuned to each  
552 study's purpose.  $U$  is a statistic that directly comments on the chance of two extreme events in a season, as in  
553 some stress tests for insurers (Bank of England, 2022). It could also be used to force dependency between

554 independently derived (i.e., uncorrelated) event sets at selected percentile(s) (e.g. 75<sup>th</sup>, 95<sup>th</sup>, 99<sup>th</sup>) perhaps with  
555 copulas (e.g., Hillier et al., 2023) to better estimate actual likely losses, improving on using one Spearman's  $r$   
556 value to represent dependency for all events causing notable losses (Hillier et al., 2024). Given these apparent  
557 discrepancies, it would be beneficial to further investigate extreme winds and high river flows or flooding,  
558 perhaps with larger model ensembles.

559

#### 560 4.2. Co-occurrence across timeframes

561

562 How does strength of co-occurrence vary with the time-window ( $\Delta t$ ) used to group events? Previous wind-flow  
563 work using Spearman's  $r$  on regular, non-overlapping periods found it to increase for windows of up to 20-40  
564 days and then hold steady, perhaps decreasing slightly for a whole season (Bloomfield et al., 2023). Fig. 5,  
565 however, uses a measure of tail dependency to focus on the severe events ( $\varepsilon_j^{75}$ ) thought to best represent  
566 impactful events (Bloomfield et al. (2023), Appendix A.4), and indicates that uplift ( $U$ ) is highest for shorter  
567 time windows. Assuming UKCP18 correctly captures persistence, this overturns the working hypothesis in the  
568 initial papers (Hillier et al., 2015; Hillier and Dixon, 2020). These looked at seasonal timescales, as the prevailing  
569 yet unpublished view in 2015 was that individual storms were either wet or windy, and took evidence of wet  
570 and stormy winters (Kendon and McCarthy, 2015; Matthews et al., 2014) to indicate that co-occurrence might  
571 most strongly exhibit on long timescales ( $\Delta t = 180$ ). Descriptively and numerically, understanding this trend in  
572 strength of dependence with timeframe is useful for stakeholders who might have varied elements of their  
573 business to risk assess, from operational (e.g. 3 day or 21 day long event durations in insurance contracts, or  
574 railway repairs) to planning (e.g. annual regulatory or budgetary).

575

576 Understanding the relative dominance and interplay of the various hydrometeorological processes is less  
577 readily achieved. The conceptual, multi-temporal model set out by Bloomfield et al (2023) details evidence for  
578 shorter-term ( $\Delta t \approx 1-15$  days) contributions from storms (i.e. sub-storm to storm clusters) and longer term  
579 'memory', perhaps in GB groundwater or distant conditions (De Luca et al., 2017; Hillier et al., 2015) mediated  
580 by atmospheric behaviours captured by weather patterns or the NAO index (Bloomfield et al., 2024; e.g., Hillier  
581 et al., 2020). Whilst winters in GB and NW Europe can be undoubtably wet and stormy (Met Office, 2024), the  
582 pattern in Fig. 5 adds weight to a case that processes at shorter timescales of a few weeks or less might  
583 dominate (i.e. storms, or storm sequences) rather than a set of conditions established for a season (e.g. Arctic  
584 sea-ice) dominating. But, any definite statement still seems premature. To aid progression to a process-  
585 orientated view, future statistical simulation modelling to split out contributions at the various time-scales  
586 (e.g., Hillier and Dixon, 2020) with a consistent metric (e.g.  $\chi$ ,  $U$ ,  $r$ ) is needed for high-flows and extreme wind.  
587 Meanwhile, a more in-depth look at the jet stream states associated with extreme winds and high flows can  
588 also contribute.

589

#### 4.3. Utility of simple jet stream metrics

590

591

592 Extra-tropical cyclone (ETC) development is closely intertwined with the jet stream (Clark and Gray, 2018;  
593 Dacre and Pinto, 2020; e.g., Geng and Sugi, 2001; Laurila et al., 2021). Illustratively, windstorms are located on  
594 its poleward side and are more intense when the jet is stronger (Laurila et al., 2021), and ETC clustering is more  
595 intense in GB with a strong persistent jet at  $\sim 50^\circ\text{N}$  (Pinto et al., 2014; Priestley et al., 2017). So, it was logical for  
596 Hillier and Dixon (2020) to propose the jet stream had a role in whether flooding and extreme wind co-occur or  
597 not based on an ETCs relationship with the jet.

598

599 Practically, calculating an index to quantify the jet stream (Ayres and Screen, 2019; e.g., Woolings et al., 2010;  
600 Zappa et al., 2018) is less demanding than cyclone tracking (e.g., Hoskins and Hodges, 2002; Manning et al.,  
601 2024). So it is useful to ask if the relatively simply derived metrics for the eddy-driven (lower tropospheric)  
602 North Atlantic jet of Woolings et al. (2010) can be a functional, readily applied tool to distinguish co-  
603 occurrence. If so, by being computationally easier than running cyclone tracking algorithms, it should facilitate  
604 inter-comparison of this potential driver of co-occurring high-flows and extreme wind between climate models  
605 and reanalyses (e.g. CMIP6, ERA5, UKCP18).

606

607 Fig. 7 (panels a,b,d and e) clearly shows that the jet stream index of Woolings et al. (2010) is able to distinguish  
608 different large-scale jet dynamics associated with joint high-flow and wind events ( $\varepsilon_J^{75}$ , dark red line), providing  
609 an easy answer to the question posed about utility. Specifically, wind ( $\varepsilon_W^{95}$ ) and  $\varepsilon_J^{75}$  episodes have a stronger  
610 jet than high-flows ( $\varepsilon_F^{95}$ ), in accord with analysis of extreme precipitation and expectations that a weaker jet  
611 causes ETCs to move more slowly allowing rainfall to persist for longer (Hillier and Dixon, 2020; Manning et al.,  
612 2024). Indeed, Fig. 7 demonstrates how statistical significance testing using jet metrics can lend support this  
613 idea, augmenting visual analysis (Manning, 2024). In future (2061-2079) latitude illustrates a case where  
614 signatures of subsets are similar, with distinctions not clear-cut using only this index (Fig. 7c). So other views,  
615 such as on the timing of episodes within a season or their planform distributions of associated high-level wind  
616 (Fig. 6, Fig. 8), are also useful to understand the influence of the jet stream.

617

#### 4.4. Potential influences of the jet stream on future co-occurrence

618

619

620 Do dynamical (e.g. jet stream) or thermodynamic effects most control the co-occurrence? Previous analysis has  
621 inferred that the future increase in co-occurrence is a predominantly thermodynamic response (i.e. warmer air  
622 can be wetter, and therefore more high FSI events), assisted by southwards displaced cyclone tracks leading to  
623 dynamically enhanced temperature (Manning et al., 2024). Fig. 6-8 allows this to be clarified.

624

625 First, consider 21 day episodes (Fig. 6a-c), likely associated with storm sequences (e.g., Bloomfield et al., 2023;  
626 Dacre and Pinto, 2020; Mühr et al., 2022). For a start, simply doubling the number of high-flow events during  
627 Oct-Mar in a wetter future world is insufficient ( $R_{\text{day}}$ , Fig. 6c). Interestingly, both high-flows and wind extremes  
628 become more seasonal, focused into midwinter, particularly and higher percentiles of FSI (Fig. 6a,d, Appendix  
629 A). An increased frequency of high flows across winter as a whole is an established idea (Griffin et al., 2022b),  
630 but within this the increased seasonality has not been noticed as the only relevant study lacked data over NW  
631 Europe (Ridder et al., 2020). Logically this phenomenon forces future co-occurrences to be more focussed in  
632 Jan (Fig. 6c,f), and when this more intense seasonality is isolated and modelled ( $R_{\text{year}}$ ) it is nearly possible to  
633 explain the UKCP18 events (dark red line). So, at this timeframe, *if* atmospheric drivers distribute extreme  
634 conditions correctly by month, thermodynamics are nearly sufficient to explain the increase in co-occurrence in  
635 future. Fig. 7b,c demonstrates that mean UKCP18 jet stream latitude becomes more seasonal in future, in  
636 wintertime shifting south (equatorwards) and focussing on 45°N to impact GB. A stronger and squeezed future  
637 jet is in line with CMIP simulations (Oudar et al., 2020; Peings et al., 2018), so a latitudinally squeezed  
638 wintertime jet might be the key dynamical driver of the increasingly seasonal future uptick in joint events. A  
639 equatorwards shift is in line with the Polar Amplification Model Intercomparison Project (PAMIP) findings  
640 where a sea-ice loss effect outweighs the polewards shift in the jet due to oceanic warming in this ‘tug-of-war’  
641 (Screen et al., 2022). A northwards historical (1979–2019) shift of the jet stream has been reported in  
642 reanalysis products and climate model runs for the present day (inc. UKCP18), inferred from a difference  
643 between mean zonal wind velocity (500 hPa) at 40–50°N as compared to 20–30°N (Woolings et al., 2023). This,  
644 however, is readily reconciled with our finding of a potential future southerly shift in the jet and that of ETC  
645 tracks (Manning, 2024), by considering Fig. 6b,c. In DJF, in the Atlantic at least, there is a *southwards* shift of  
646 the jet *into* the 40–50°N bin, increasing typical wind speeds there with respect to that at 20–30°N. So, Fig. 6  
647 provides an additional insight into how broad-scale thermodynamic and dynamic factors combine to explain  
648 longer joint high-flow and wind episodes.

649

650 For individual or closely consecutive storms ( $\Delta t = 3$  days), Fig. 6e,f clearly shows that the number of events  
651 alone is insufficient to cause the co-occurrences in UKCP18, particularly in the future, even if enhanced  
652 seasonality is accounted for (red line,  $R_{\text{year}}$ ). So, another shorter-term explanatory atmospheric behaviour is  
653 needed. Fig. 7 and Fig. 8 suggest that this is the disposition and dynamics of the jet stream. In terms of the  
654 latitude and speed of the jet’s strongest part, the typical mid-winter jet becomes more like that characteristic  
655 of impactful compound storms today (Fig. 7). Fig. 8 adds plan-view information on the jet at the time of high  
656 joint FSI-SSI episodes impact GB. In the present, joint episodes ( $\varepsilon_j^{75}$ ) have a jet that typically blends most of the  
657 strength of wind events ( $\varepsilon_W^{95}$ ) with the more southerly track of high-flow inducing events ( $\varepsilon_F^{95}$ ). In future, a  
658 stronger and more southerly jet is much more prominent for  $\varepsilon_j^{75}$  episodes (Fig. 7c, Fig. 8e), fitting with the

659 location of extreme precipitation (Bloomfield et al., 2024) and its associated jet (Manning et al., 2024) moving  
660 south.

661

662 Future high FSI-SSI episodes ( $\epsilon_j^{75}$ ) more resemble wind episodes than high-flow (Fig. 8d-f), fitting with a view of  
663 a typically rainy wintertime future GB where wind is typically the missing element for a joint event (Bloomfield  
664 et al., 2024). Namely, wind becomes the limiting factor rather than flooding as it is now; currently multi-basin  
665 high-flows needs multiple storms setting wet antecedent conditions (De Luca et al., 2017), and locally the joint  
666 impact footprint's extent is limited by its rain component (Manning et al., 2024). Intriguingly, a southerly jet  
667 anomaly during a compound storm's lifetime over the Atlantic (Fig. A1 - Manning et al., 2024) that obtains a  
668 very windy signature when impacting GB (Fig. 8d,f) suggests the most severe future events might arise from a  
669 jet initially passing over warm southerly water that strengthens and shifts north as it impacts southern GB. So,  
670 in a modification to the conclusion of Manning et al. (2024) a relatively equal contribution of dynamics (i.e. jet  
671 disposition and seasonality) and thermodynamical (i.e. warmer air carries more moisture) is argued to drive  
672 future increases in joint hazard in GB.

673

674 Placing an emphasis on dynamics (e.g. jet stream) ties in with a broader, emerging picture of linked multi-  
675 hazards across the Atlantic domain (e.g., Röthlisberger et al., 2016). Cold air outbreaks over eastern Canada  
676 followed by wind extremes over northern Europe and the British Isles appear associated with an enhanced jet  
677 stream (Leeding et al., 2023), whilst January being the dominant month for compound surge and rainfall  
678 around GB (Bevacqua et al., 2020) ties to the same timing for wind and riverine high-flows (Fig. 6).  
679 Furthermore, clustered ETC are associated with a jet stream anomaly focussed on GB (Dacre and Pinto, 2020;  
680 Pinto et al., 2014; Priestley et al., 2017). And, like flow regimes globally, these relationships are likely to change  
681 with the climate (e.g., Jiménez Cisnero and Oki, 2014; Li et al., 2024). We therefore advocate a process-  
682 orientated approach to co-occurring hazards (e.g., Manning et al., 2024) and highlight that the 'recipe' of  
683 driving large-scale conditions (e.g. jet stream state) for a 'perfect storm' will vary by country (Gonçalves et al.,  
684 2023; Raveh-Rubin, 2015; Röthlisberger et al., 2016)

685

## 686 **5. Conclusions**

687

688 This study uses novel statistical modelling of dependencies and a jet stream index (Woolings et al., 2010) to  
689 understand the co-occurrence of high-flows and extreme wind events in multi-hazard *episodes*, with a focus on  
690 3-day and 21-day durations. The idea of dynamically defined episodes that group events to reflect periods of  
691 adverse conditions is defined to reflect lived experience, and extracted using the FSI (Bloomfield et al., 2023,  
692 2024) and SSI indices (e.g., Klawa and Ulbrich, 2003) from the UKCP18 regional 12km dataset which has  
693 previously been validated (Bloomfield et al., 2023). The main conclusions are:

694

- 695 • Defining stormy multi-event episodes as they are experienced (i.e. dynamically positioned time  
696 windows) produces results that align with previous work, giving stakeholders additional comfort in  
697 using published results.
- 698 • This said, statistically, it is critical to note that different dependency measures (e.g.  $\chi$ ,  $U$ ,  $r$ ,  $\tau$ ) reflect  
699 different aspects of distributions of joint extremes, and may even appear contradictory. Also, using  
700 fixed timeframe for analysis (e.g. Oct-Mar, DJF) should be used with caution, especially since peak  
701 months may shift in future. Statistically modelling seasonality in a month-by-month analysis as done  
702 here may be necessary.
- 703 • Uplift ( $U$ ) in co-occurrence is found to increase as severity increases (e.g. 90<sup>th</sup> to 99<sup>th</sup> percentile),  
704 meaning that evidence is starting to suggest that dependence exists to high return periods, even if not  
705 strictly 'asymptotic'. So, ignoring correlation underestimates risk most for the strongest storms.
- 706 • Uplift is found to increase as  $\Delta t$  is reduced, highest within insurers' key windows ( $\Delta t = 3,21$  days),  
707 suggesting the importance of atmospheric mechanisms that act to drive co-occurrence at timescales of  
708 days to weeks (e.g. storm sequences); see the framework model in Bloomfield et al. (2023). So,  
709 ignoring correlation underestimates risk most for individual or closely grouped storms.
- 710 • Jet stream metrics (e.g., Woolings et al., 2010) are found to be a useful, easily determined tool to  
711 investigate its roles as a driver of co-occurrence.
- 712 • Future strong jet streams become increasingly focused in mid-winter (Dec-Feb) driving the increased  
713 seasonality in individual hazards, a larger effect for more extreme events. This broad-scale dynamic  
714 effect, combined with thermodynamics (i.e. a warmer, wetter world), explains most of the uplift in  
715 future joint events at storm-sequence timescales ( $\Delta t = 21$  days) and over.
- 716 • For individual or closely consecutive storms ( $\Delta t = 3$  days), altered jet characteristics are also needed to  
717 fully explain the uplift in co-occurrence, stronger and displaced southwards as storms impact GB. In  
718 short, typical future DJF jet variability closely resembles that of impactful compound storms in GB  
719 today highlighting the contribution of the jet changes to the increase in extremes.

720

721 Future work will could unpick and quantify the balance between dynamic and thermodynamic effects, ideally  
722 using higher resolution data from a variety of climate models. It will be important, however, to build area-by-  
723 area understanding of how the impact of common drivers varies spatially to improve risk mitigation and  
724 planning (e.g. diversification, mutual aid across Europe). As the jet stream guides storms to one country,  
725 another will be spared.

726

727

728

#### **Conflict of interest statement**

729

730 No conflicts of interest.

731

## 732 **Acknowledgements**

733

734 To undertake this work Hillier was funded by a NERC, UK Knowledge Exchange Fellowship (Grant Number  
735 NE/V018698/1). Bloomfield, Shaffrey, Bates and Kumar are part-supported by the UK Centre for Greening  
736 Finance and Investment (NERC CGFI Grant Number NE/V017756/1), which Hillier is associated with as an  
737 Associate Research Fellow. Thanks are given to Adam Griffin at CEH and the AquaCAT project, who developed  
738 the UKCP18 based river flow simulations, advised about them and provided a daily time-series to accompany  
739 them.

740

## 741 **Authors' contributions**

742

743 The work was conceived by JH with input from HB, PB, LS. Analysis was by JH, with input from HB. Writing and  
744 interpretation was led by JH with input from all authors. DK created Fig. 1.

745

## 746 **Data availability statement**

747

748 UKCP18 data are available from the Met Office. Flooding events are from Griffin *et al* (2022a) on the CEDA  
749 repository. Wind events will be made available on CEDA.

750

## 751 **6. References**

752

753 Ayres, H. C. and Screen, J. A.: Multimodel analysis of the atmospheric response to Antarctic sea ice loss at  
754 quadrupled CO<sub>2</sub>, *Geophysical Research Letters*, 46, 9861–9869, <https://doi.org/10.1029/2019GL083653>, 2019.

755 Bank of England: General Insurance Stress Test 2022, 2022.

756 Berghuijs, W. R., Harrigan, S., Molnar, P., Slater, L., and Kirchner, J. W.: The relative importance of different  
757 flood-generating mechanisms across Europe, *Water Resour. Res.*, 55, 4582–4593,  
758 <https://doi.org/10.1029/2019WR024841>, 2019.

759 Bevacqua, E., Maraun, D., Haff, H. I., Widmann, M., and Vrac, M.: Multivariate statistical modelling of  
760 compound events via pair-copula constructions: analysis of floods in Ravenna (Italy), *Hydrol. Earth Syst. Sci.*, 21,  
761 2701–2723, 2017.

762 Bevacqua, E., Vousdoukas, V. I., Zappa, G., Hodges, K., Shepherd, T. G., Maraun, D., Mentaschi, L., and Feyen, L.:  
763 More meteorological events that drive compound coastal flooding are projected under climate change,  
764 *Communications Earth and Environment*, 1, 47, <https://doi.org/10.1038/s43247-020-00044-z>, 2020.

- 765 Bevacqua, E., De Michele, C., Manning, C., Couasnon, A., Ribeiro, A. F. S., Ramos, A. M., Vignotto, E., Bastos, A.,  
766 Blesic, S., Durante, F., Hillier, J. K., Oliveira, S. C., Pinto, J. G., Ragno, E., Rivoire, P., Saunders, K., van der Wiel, K.,  
767 Wu, W., Zhang, T., and Zscheischler, J.: Guidelines for Studying Diverse Types of Compound Weather and  
768 Climate Events, *Earth's Future*, 9, e2021EF002340, <https://doi.org/10.1029/2021EF002340>, 2021.
- 769 Bister, M. and Emanuel, K.: Dissipative Heating and Hurricane Intensity, *Meteorology and Atmospheric Physics*,  
770 65, 233–240, 1998.
- 771 Black, A. R. and Law, F. M.: Development and utilization of a national web-based chronology of hydrological  
772 events/Développement et utilisation sur internet d'une chronologie nationale d'événements hydrologiques.,  
773 *Hydrological Sciences Journal*, 49, 237–246, <https://doi.org/10.1623/hysj.49.2.237.34835>, 2004.
- 774 Bloomfield, H., Hillier, J. K., Griffin, A., Kay, A. L., Shaffrey, L., Pianosi, F., James, R., Kumar, D., Champion, A. J.,  
775 and Bates, P. D.: Co-occurring wintertime flooding and extreme wind over Europe, from daily to seasonal  
776 timescales, *Weather Clim. Extremes*, 39, 100550, <https://doi.org/10.1016/j.wace.2023.100550>, 2023.
- 777 Bloomfield, H. C., Bates, P. D., Schaffrey, L. C., Hillier, J. K., Champion, A., Cotterill, D., Pope, J. O., and Kumar, D.:  
778 Synoptic conditions conducive for compound wind-flood events in Great Britain in present and future climates,  
779 *Env. Res. Lett.*, 19, 024019, <https://doi.org/10.1088/1748-9326/ad1cb7>, 2024.
- 780 Böllman, G. and Jurksch, G.: Ein Beitrag zur Festlegung der Grundwind- und Nennböengeschwindigkeit im  
781 Binnenland der Bundesrepublik Deutschland für die DIN-NORM 1055, Teil 4, *Meteorol. Rdsch.*, 37, 1–10, 1984.
- 782 Businger, S. and Businger, J.: Viscous Dissipation of Turbulence Kinetic Energy in Storms, *Journal of the*  
783 *Atmospheric Sciences*, 58, 3793–3796, 2001.
- 784 CCC: Copernicus Climate Change Service (C3S), Climate Data Store (CDS), (2022): Winter windstorm indicators  
785 for Europe from 1979 to 2021 derived from reanalysis, <https://doi.org/10.24381/cds.9b4ea013>, 2022.
- 786 Champion, A. J., Allan, R. P., and Lavers, D. A.: Atmospheric rivers do not explain UK summer extreme rainfall,  
787 *Journal of Geophysical Research: Atmospheres*, 120, 6731–6741, <https://doi.org/10.1002/2014JD022863>,  
788 2015.
- 789 Chandler, A. M., Jones, E. J. W., and Patel, M. H.: Property loss estimation for wind and earthquake perils, *Risk*  
790 *Analysis*, 21, 235–249, <https://doi.org/10.1111/0272-4332.212108>, 2001.
- 791 Christofides, S., Barlow, C., Michaelides, N., and Miranthis, C.: Storm Rating in the Nineties, 1992 General  
792 Insurance Convention, 18th Nov 1992, 5–89, 1992.
- 793 Claassen, J., Ward, P. J., Daniell, J. E., Koks, E. E., Tiggeloven, T., and de Ruiter, M. C.: A new method to compile  
794 global multi-hazard event sets, *Scientific Reports*, 13, 13808, <https://doi.org/10.1038/s41598-023-40400-5>,  
795 2023.
- 796 Clark, P. A. and Gray, S. L.: Sting jets in extratropical cyclones: a review, *Quart. J. Royal Meteorol. Soc.*, 148, 943–  
797 969, <https://doi.org/10.1002/qj.3267>, 2018.
- 798 Coles, S., Heffernan, J., and Tawn, J.: Dependence measures for extreme value analyses, *Extremes*, 2, 339–365,  
799 <https://doi.org/10.1023/A:1009963131610>, 1999.
- 800 Collet, L., Harrigan, S., Prudhomme, C., Formetta, G., and Beevers, L.: Future hot-spots for hydro-hazards in  
801 Great Britain: A probabilistic assessment, *Hydrol. Earth Syst. Sci.*, 22, 5387–5401, [https://doi.org/10.5194/hess-](https://doi.org/10.5194/hess-22-5387-2018)  
802 [22-5387-2018](https://doi.org/10.5194/hess-22-5387-2018), 2018.

803 Cotterill, D., Stott, P., Christidis, N., and Kendon, E.: Increase in the frequency of extreme daily precipitation in  
804 the United Kingdom in autumn, *Weather Clim. Extremes*, 33, 100340,  
805 <https://doi.org/10.1016/j.wace.2021.100340>, 2021.

806 Dacre, H. F. and Pinto, J. G.: Serial clustering of extratropical cyclones: a review of where, when and why it  
807 occurs, *npj Climate and Atmospheric Science*, 3, <https://doi.org/10.1038/s41612-020-00152-9>, 2020.

808 De Luca, P., Hillier, J. K., Wilby, R. L., Quinn, N. W., and Harrigan, S.: Extreme multi-basin flooding linked with  
809 extra-tropical cyclones, *Env. Res. Lett.*, 12, 114009, <https://doi.org/10.3390/atmos10100577>, 2017.

810 Dixon, R., Souch, C., and Whitaker, D.: European windstorm: Needs of the insurance industry, in:  
811 <http://www.stormworkshops.org/workshop2017.html>, Reading, UK. 21-23 June 2017., 2017.

812 Donges, J. F., Schleussner, C. F., Siegmund, J. F., and Donner, R. V.: Event coincidence analysis for quantifying  
813 statistical interrelationships between event time series, *Eur. Phys. J. Special Topics*, 225, 471–487,  
814 <https://doi.org/10.1140/epjst/e2015-50233-y>, 2016.

815 Dorland, C., Tol, R. S. J., and Palutikof, J.: Vulnerability of the Netherlands and northwest Europe to storm  
816 damage under climate change, *Climate Change*, 43, 513–535, 1999.

817 Emanuel, K.: The power of a hurricane: An example of reckless driving on the information superhighway,  
818 *Weather*, 54, 107–108, 1998.

819 Emanuel, K.: Increasing destructiveness of tropical cyclones over the past 30 years, *Nature*, 436, 686–688, 2005.

820 Escobar, M.: Studying coincidences with network analysis and other multivariate tools, *The Stata Journal*, 15,  
821 1118–1156, 2015.

822 Fink, A. H., Brucher, T., Ermert, V., Kruger, A., and Pinto, J. G.: The European storm Kyrill in January 2007:  
823 Synoptic evolution, meteorological impacts and some considerations with respect to climate change, *Nat.*  
824 *Hazards Earth Syst. Sci.*, 9, 405–423, 2009.

825 Gallina, V., Torresan, S., Critto, A., Sperotto, A., Glade, T., and Marcomini, A.: A review of multi-risk  
826 methodologies for natural hazards: Consequences and challenges for a climate change impact assessment,  
827 *Journal of Environmental Management*, 168, 123–132, <https://doi.org/10.1016/j.jenvman.2015.11.011>, 2016.

828 Geng, Q. and Sugi, M.: Variability of the North Atlantic Cyclone Activity in Winter Analyzed from NCEP–NCAR  
829 Reanalysis Data, *Journal of Climate*, 14, 3863–3873, 2001.

830 Gonçalves, A. C. R., Nieto, R., and Liberato, M. L. R.: Synoptic and Dynamical Characteristics of High-Impact  
831 Storms Affecting the Iberian Peninsula during the 2018–2021 Extended Winters, *Atmosphere*, 14, 1353,  
832 <https://doi.org/10.3390/atmos14091353>, 2023.

833 Griffin, A., Kay, A., Bell, V., Stewart, E., Sayers, P., and Carr, S.: Peak flow and probability of exceedance data for  
834 grid-to-grid modelled widespread flooding events across mainland GB from 1980–2010 and 2050–2080,  
835 <https://doi.org/10.5285/26ce15dd-f994-40e0-8a09-5f257cc1f2ab>, 2022a.

836 Griffin, A., Kay, A. L., Sayers, P., Bell, E., and Carr, S.: Widespread flooding dynamics changing under climate  
837 change: characterising floods using ukcp18, *Hydrol. Earth Syst. Sci. Discussions*, 1–18,  
838 <https://doi.org/10.5194/hess-2022-243>, 2022b.

839 Hadzilicos, G., Li, R., Harrington, P., Latchman, S., Hillier, J. K., Dixon, R., New, C., Alabaster, A., and Tsapko, T.: It's  
840 windy when it's wet: why UK insurers may need to reassess their modelling assumptions, *Bank Underground*,  
841 2021.

- 842 Harrigan, S., Zoster, E., Cloke, H., Salamon, P., and Prudhomme, C.: Daily ensemble river discharge reforecasts  
843 and real-time forecasts from the operational global flood awareness system., 27, 1–19,  
844 <https://doi.org/10.5194/hess-27-1-2023>, 2023.
- 845 Heffernan, J. and Tawn, J.: A conditional approach for multivariate extreme values, *J. R. Statistic. Soc. B*, 66,  
846 169–182, 2004.
- 847 Heneka, P. and Ruck, B.: A damage model for the assessment of storm damage to buildings, *Engineering*  
848 *Structures*, 30, 3603–3609, <https://doi.org/10.1016/j.engstruct.2008.06.005>, 2008.
- 849 Heneka, P., Hofherr, T., Ruck, B., and Kottmeier, C.: Winter storm risk of residential structures – model  
850 development and application to the German state of Baden-Württemberg, *Natural Hazards and Earth System*  
851 *Science*, 6, 721–733, <https://doi.org/10.5194/nhess-6-721-2006>, 2006.
- 852 Hersbach, H., Bell, B., Berrisford, P., Hirihana, S., Horányi, A., Muñoz-Sabater, J., Nicolas, J., Peubey, C., Radu, R.,  
853 and Schepers, D.: The ERA5 global reanalysis, *Q. J. R. Meteorol. Soc.*, 146, 1999–2049, [https://doi.org/10.](https://doi.org/10.1002/qj.3803)  
854 [1002/qj.3803](https://doi.org/10.1002/qj.3803), 2020.
- 855 Hewitt, K. and Burton, I.: *Hazardousness of a place: a regional ecology of damaging events*, Toronto Press,  
856 Toronto, 154 pp., 1971.
- 857 Hewston, R. and Dorling, S. R.: An analysis of observed daily maximum wind gusts in the UK, *Journal of Wind*  
858 *Engineering and Industrial Aerodynamics*, 99, 845–856, <https://doi.org/10.1016/j.jweia.2011.06.004>, 2011.
- 859 Hill, M., Gatley, D., and Peiris, N.: Damage observations in the UK from Windstorm Ulli and implications for  
860 building codes and loss estimation, 6th European and African Conference on Wind Engineering, 7th - 14th July  
861 2013, Cambridge, UK, 1–8, 2013.
- 862 Hillier, J. K.: The Perils in Brief, in: *Natural Catastrophe Risk Management and Modelling: A Practitioner’s Guide*,  
863 Wiley-Blackwell, Oxford, UK, pp 536, 2017.
- 864 Hillier, J. K. and Dixon, R.: Seasonal impact-based mapping of compound hazards, *Env. Res. Lett.*, 15, 114013,  
865 <https://doi.org/10.1088/1748-9326/abbc3d>, 2020.
- 866 Hillier, J. K. and Van Meeteren, M.: Co-RISK: A tool to co-create impactful university-industry projects for  
867 natural hazard risk mitigation, *Geosci. Commun.*, 7, 35–56, <https://doi.org/10.5194/gc-7-35-2024>, 2024.
- 868 Hillier, J. K., Macdonald, N., Leckebusch, G. C., and Stavriniades, A.: Interactions between apparently primary  
869 weather-driven hazards and their cost, *Env. Res. Lett.*, 10, 104003, [https://doi.org/doi:10.1088/1748-](https://doi.org/doi:10.1088/1748-9326/10/10/104003)  
870 [9326/10/10/104003](https://doi.org/doi:10.1088/1748-9326/10/10/104003), 2015.
- 871 Hillier, J. K., Matthews, T., Wilby, R. L., and Murphy, C.: Multi-hazard dependencies can increase and decrease  
872 risk, *Nature Climate Change*, 10, 595–598, <https://doi.org/10.1038/s41558-020-0832-y>, 2020.
- 873 Hillier, J. K., Perkins, T., Li, R., Bloomfield, H., Lau, J., Claus, S., Harrington, P., Latchman, S., and Humphry, D.:  
874 What if it’s a perfect storm? Stronger evidence that insurers should account for co-occurring weather hazards,  
875 *Bank Underground*, 2023.
- 876 Hillier, J. K., Champion, A., Perkins, T., Garry, F., and Bloomfield, H.: GC Insights: Open R-code to communicate  
877 the impact of co-occurring natural hazards, *Geoscience Communication Discussions*,  
878 <https://doi.org/10.5194/egusphere-2023-2799>, 2024.
- 879 Hirpa, F. A., Salamon, P., Beck, H. E., Lorini, V., Alfieri, L., Zoster, E., and Dadson, S. J.: Calibration of the Global  
880 Flood Awareness System (GloFAS) using daily streamflow data, *Journal of Hydrology*, 566, 595–606, 2018.

- 881 Hoskins, B. and Hodges, K.: New perspectives on the Northern Hemisphere winter storm tracks, *Journal of*  
882 *Atmospheric Sciences*, 59, 1041–1061, 2002.
- 883 Jacob, D., Petersen, J., Eggert, B., Alias, A., Christensen, O. B., Bouwer, L. M., Braun, A., Colette, A., Déqué, M.,  
884 and Georgievski, G.: EURO-CORDEX: new high-resolution climate change projections for European impact  
885 research, *Reg. Environ. Change*, 14, 563–578, <https://doi.org/10.1007/s10113-013-0499-2>, 2014.
- 886 Jiménez Cisnero, B. E. and Oki, T.: Part A: Global and Sectoral Aspects. Contribution of Working Group II to the  
887 Fifth Assessment Report of the Intergovernmental Panel on Climate Change, in: *Climate Change 2014: Impacts,*  
888 *Adaptation, and Vulnerability*, Cambridge University Press, Cambridge, UK, 229–269, 2014.
- 889 Jones, T., Stephenson, D. B., and Priestley, M. K.: Correlation of wind and precipitation annual aggregate  
890 severity of European cyclones, *Weather*, <https://doi.org/10.1002/wea.4573>, 2024.
- 891 Kappes, M. S., Keiler, M., von Elverfeldt, K., and Glade, T.: Challenges of analyzing multi-hazard risk: a review,  
892 *Nat. Hazards*, 64, 1925–1958, <https://doi.org/10.1007/s11069-012-0294-2>, 2012.
- 893 Kay, A., Griffin, A., Rudd, A., Chapman, R., Bell, V., and Arnell, N.: Climate change effects on indicators of high  
894 and low river flow across Great Britain, *Adv. Water Resour.*, 151, 103909,  
895 <https://doi.org/10.1016/j.advwatres.2021.103909>, 2021.
- 896 Kendon, M.: Storms Dudley, Eunice and Franklin February 2022., Technical Report. Met Office., 2022.
- 897 Kendon, M. and McCarthy, M.: The UK’s wet and stormy winter of 2013/2014, *Weather*, 7, 40–47, 2015.
- 898 Klawa, M. and Ulbrich, U.: A model for the estimation of storm losses and the identification of severe winter  
899 storms in Germany, *Nat. Hazards Earth Syst. Sci.*, 3, 725–732, 2003.
- 900 Kopp, J., Rivoire, P., Ali, S. M., Barton, Y., and Martius, O.: A novel method to identify sub-seasonal clustering  
901 episodes of extreme precipitation events and their contributions to large accumulation periods, *Hydrol. Earth*  
902 *Syst. Sci.*, 25, 5153–5174, <https://doi.org/10.5194/hess-25-5153-2021>, 2021.
- 903 Küpfer, K.: Impact-based event catalogue on serially clustered extreme events of different types in south-west  
904 Germany, 2024.
- 905 Lane, R. A. and Kay, A. L.: Climate change impact on the magnitude and timing of hydrological extremes across  
906 Great Britain, *Frontiers in Water*, 71, 684982, <https://doi.org/10.3389/frwa.2021.684982>, 2021.
- 907 Laurila, T. K., Gregow, H., Cornér, J., and Sinclair, V. A.: Characteristics of extratropical cyclones and precursors  
908 to windstorms in northern Europe, *Weather and Climate Dynamics*, 2, 1111–1130,  
909 <https://doi.org/10.5194/wcd-2-1111-2021>, 2021.
- 910 Lechner, J. A., Simiu, E., and Heckert, N. A.: Assessment of ‘peaks over threshold’ methods for estimating  
911 extreme value distribution tails, *Structural Safety*, 12, 305–314, [https://doi.org/10.1016/0167-4730\(93\)90059-](https://doi.org/10.1016/0167-4730(93)90059-A)  
912 *A*, 1993.
- 913 Leckebusch, G. C., Renggli, D., and Ulbrich, U.: Development and Application of an Objective Storm Severity  
914 Measure for the Northeast Atlantic Region, *Meteorologische Zeitschrift*, 17, 575–587,  
915 <https://doi.org/10.1127/0941-2948/2008/0323>, 2008.
- 916 Leeding, R., Riboldi, J., and Messori, G.: On Pan-Atlantic cold, wet and windy compound extremes, *Weather*  
917 *Clim. Extremes*, 39, 100524, <https://doi.org/10.1016/j.wace.2022.100524>, 2023.

- 918 Li, D., Zscheischler, J., Chen, Y., Yin, B., Feng, J., Freud, M., Qi, J., Zu, Y., and Bevacqua, E.: Intensification and  
919 Poleward Shift of Compound Wind and Precipitation Extremes in a Warmer Climate, *Geophys. Res. Lett.*, 51,  
920 <https://doi.org/10.1029/2024GL110135>, 2024.
- 921 Liberato, M. L. R.: The 19 January 2013 windstorm over the North Atlantic: Large-scale dynamics and impacts  
922 on Iberia, *Weather Clim. Extremes*, 5–6, 16–28, <https://doi.org/10.1016/j.wace.2014.06.002>, 2014.
- 923 Lockwood, J., Guentchev, G. S., Alabaster, A., Brown, S. J., Palin, E. J., Roberts, M. J., and Thronton, H. E.: Using  
924 high-resolution global climate models from the PRIMAVERA project to create a European winter windstorm  
925 event set, *Nat. Hazards Earth Syst. Sci.*, 22, 3585–3606, <https://doi.org/10.5194/nhess-22-3585-2022>, 2022.
- 926 Lowe, J. A., Bernie, D., Bett, P., Bircheno, L., Brown, S., Calvert, D., Clarke, R., Eagle, K., Edwards, T., and Fosser,  
927 G.: UKCP18 Science Overview Report, Met Office, Hadley Centre, Exeter, UK, 2018.
- 928 Lowe, J. A., Bernie, D., Bett, P., Brichenon, L., Brown, S., Calvert, D., Clark, R., and Eagle, K.: UKCP18 Science  
929 Overview Report, Met Office, 2019.
- 930 Mailier, P. J., Stephenson, D. B., Ferro, C. A. T., and Hodges, K. I.: Serial Clustering of Extratropical Cyclones,  
931 *Monthly Weather Review*, 134, 2224–2240, <https://doi.org/10.1175/MWR3160.1>, 2006.
- 932 Manning, C., Kendon, E. J., Fowler, H. J., Roberts, N. M., Berthou, S., Suri, D., and Roberts, N. J.: Extreme  
933 windstorms and sting jets in convection-permitting climate simulations over europe., *Climate Dynamics*,  
934 <https://doi.org/10.1007/s00382-021-06011-4>, 2022.
- 935 Manning, C., Kendon, E. J., Fowler, H. J., and Roberts, N. M.: Projected increase in windstorm severity and  
936 contribution from sting jets over the UK and Ireland, *Weather Clim. Extremes*, 40, 100562,  
937 <https://doi.org/10.1016/j.wace.2023.100562>, 2023.
- 938 Manning, C., Kendon, E. J., Fowler, H. J., Katto, J. L., Chan, S. C., and Sansom, P. G.: Compound wind and rainfall  
939 extremes: Drivers and future changes over the UK and Ireland, *Weather Clim. Extremes*, 44, 100673,  
940 <https://doi.org/10.1016/j.wace.2024.100673>, 2024.
- 941 Martius, O., Pfahl, S., and Chevalier, C.: A global quantification of compound precipitation and wind extremes:  
942 Compound precipitation and wind extremes, *Geophys. Res. Lett.*, 43, 7709–7714,  
943 <https://doi.org/10.1002/2016GL070017>, 2016.
- 944 Matthews, T., Murphy, C., Wilby, R. L., and Harrigan, S.: Stormiest winter on record for Ireland and UK, *Nature*  
945 *Climate Change*, 4, 738–740, <https://doi.org/doi:10.1038/nclimate2336>, 2014.
- 946 Matthews, T., Murphy, C., McCarthy, G., Broderik, C., and Wilby, R. L.: Super Storm Desmond: a process-based  
947 assessment, *Env. Res. Lett.*, 13, 014024, 2018.
- 948 McSweeney, C. and Bett, P.: UKCP European Circulation Indices: Jet Stream Position and Strength. UKCP  
949 Factsheet, Met Office, Hadley Centre, Exeter, UK, 2020.
- 950 Met Office: UK Storm Centre, Warnings and advice, 2024.
- 951 Mitchell-Wallace, K., Jones, M., Hillier, J. K., and Foote, M.: Natural Catastrophe Risk Management and  
952 Modelling: A Practitioner’s Guide, Wiley, Oxford, UK, 506 pp., 2017.
- 953 Mühr, B., Eisenstein, L., Pinto, G. J., Knippertz, P., Mohr, S., and Kunz, M.: Winter storm series: Ylenia, Zeynep,  
954 Antonia (int: Dudley, Eunice, Franklin) February 2022 (NW & Central Europe), KIT, 2022.
- 955 MunichRe: Winter storms in Europe (II): Analysis of 1999 losses and loss potentials, Munchener  
956 Ruckversicherungs-Gesellschaft, 2002.

- 957 Murphy, J., Harris, G., Sexton, D., Kendon, E., Brett, P., Clark, R., and Yamazaki, K.: UKCP18 land projections:  
958 science report., Met Office: Exeter, 2019.
- 959 Osinski, R., Lorenz, P., Kruschke, T., Voigt, M., Ulbrich, U., Leckebusch, G. C., Faust, E., Hofherr, T., and Majewski,  
960 D.: An approach to build an event set of European wind storms based on ECMWF EPS, *Nat. Hazards Earth Syst.*  
961 *Sci. Discuss.*, 16, 255–268, <https://doi.org/10.5194/nhessd-3-1231-2015>, 2016.
- 962 Oudar, T., Cattiaux, J., and Douville, H.: Drivers of the Northern extratropical eddy-driven jet change in CMIP5  
963 and CMIP6 Models, *Geophys. Res. Lett.*, 47, e2019GL086695, 2020.
- 964 Owen, L. E., Catto, J. L., Stephenson, D. S., and Dunstone, N. J.: Compound precipitation and wind extremes  
965 over europe and their relationship to extratropical cyclones, *Weather Clim. Extremes*, 33, 100342, 2021a.
- 966 Owen, L. E., Catto, J. L., Dunstone, N. J., and Stephenson, D. S.: How well can a seasonal forecast system  
967 represent three hourly compound wind and precipitation extremes over europe?, *Env. Res. Lett.*, 16, 074019,  
968 2021b.
- 969 Palutikof, J. and Skellern, A.: Storm Severity over Britain, A report to the Commercial Union General Insurance,  
970 Climatic Research Unit, School of Environmental Sciences, Univeristy of East Anglia, Norwich, UK, 1991.
- 971 Pardowitz, T., Osinski, R., Kruschke, T., and Ulbrich, U.: An analysis of uncertainties and skill in forecasts of  
972 winter storm losses, *Nat. Hazards Earth Syst. Sci.*, 16, 2391–2402, [https://doi.org/10.5194/nhess-16-2391-](https://doi.org/10.5194/nhess-16-2391-2016)  
973 2016, 2016.
- 974 Peings, Y., Cattiaux, J., Vavrus, S. J., and Magnusdottir, G.: Projected squeezing of the wintertime North-Atlantic  
975 jet, *Environmental Research Letters*, 074016, <https://doi.org/10.1088/1748-9326/aacc79>, 2018.
- 976 PERILS: EUR 3,851M – PERILS releases final industry loss estimate for February 2022 European Windstorm  
977 series, 2023.
- 978 PERILS: PERILS: Losses, 2024.
- 979 Pinto, J. G., Karremann, M. K., Born, K., Della-Marta, P. M., and Klawa, M.: Loss potentials associated with  
980 european windstorms under future climate conditions, *Climate Research*, 54, 1–20, 2012.
- 981 Pinto, J. G., Gómara, I., Masato, G., Dacre, H. F., Woolings, T., and Caballero, R.: Large-scale dynamics associated  
982 with clustering of extratropical cyclones affecting western Europe, *J. Geophys. Res.*, 119, 13–704,  
983 <https://doi.org/10.1002/2014JD022305>, 2014.
- 984 Prah, B. F., Rybski, D., Kropp, J. P., and Burghoff, O.: Applying stochastic small-scale damage functions to  
985 German winter storms, *Geophys. Res. Lett.*, 39, L06806, <https://doi.org/10.1029/2012GL050961>, 2012.
- 986 Prah, B. F., Rybski, D., Burghoff, O., and Kropp, J. P.: Comparison of storm damage functions and their  
987 performance, *Nat. Hazards Earth Syst. Sci.*, 15, 769–788, <https://doi.org/10.5149/nhess-15-769-2015>, 2015.
- 988 Priestley, M. D. K., Pinto, J. G., Dacre, H. F., and Shaffrey, L.: Rossby wave breaking, the upper level jet, and  
989 serial clustering of extratropical cyclones in western Europe, *Geophys. Res. Lett.*, 44, 514–521,  
990 <https://doi.org/10.1002/2016GL071277>, 2017.
- 991 Priestley, M. D. K., Dacre, H. F., Shaffrey, L., Hodges, K. I., and Pinto, J. G.: The role of serial European windstorm  
992 clustering for extreme seasonal losses as determined from multi-centennial simulations of high-resolution  
993 global climate model data, *Nat. Hazards Earth Syst. Sci.*, 18, 2991–3006, [https://doi.org/10.5194/nhess-18-](https://doi.org/10.5194/nhess-18-2991-2018)  
994 2991-2018, 2018.

- 995 Raveh-Rubin: Large-scale wind and precipitation extremes in the Mediterranean: A climatological analysis for  
996 1979–2012, *Q. J. R. Meteorol. Soc.*, 141, 2404–2417, <https://doi.org/10.1002/qj.2531>, 2015.
- 997 Ridder, N. N., Pitman, A. J., Westra, S., Ukkola, A., Do, H. X., Bador, M., Hirsch, A. L., Evans, J. P., Di Luca, A., and  
998 Zscheischler, J.: Global hotspots for the occurrence of compound events, *Nature Communications*, 11,  
999 <https://doi.org/10.1038/s41467-020-19639-3>, 2020.
- 1000 Roberts, J. F., Champion, A. J., Dawkins, L. C., Hodges, K. I., Shafferty, L., Stephenson, D. S., Stringer, M. A.,  
1001 Thronton, H. E., and Youngman, B. D.: The XWS open access catalogue of extreme European windstorms from  
1002 1979–2012, *Nat. Hazards Earth Syst. Sci.*, 14, 2487–2501, <https://doi.org/10.5194/nhess-14-2487-2014>, 2014.
- 1003 Robson, A. and Reed, D.: Statistical procedures for flood frequency estimation., in: *Flood Estimation Handbook*,  
1004 vol. 3, Institute of Hydrology, 338, 1999.
- 1005 Röthlisberger, M., Pfahl, S., and Martius, O.: Regional-scale jet waviness modulates the occurrence of  
1006 midlatitude weather extremes, *Geophys. Res. Lett.*, 43, 10989–10997, <https://doi.org/10.1002/2016GL070944>,  
1007 2016.
- 1008 de Ruiter, M., Couasnon, A., van den Homberg, M. J. C., Daniell, J. E., Gill, J., and Ward, P. J.: Why We Can No  
1009 Longer Ignore Consecutive Disasters, *Earth’s Future*, 8, e2019EF001425,  
1010 <https://doi.org/10.1029/2019EF001425>, 2019.
- 1011 Saville, G.: A stormy end to winter: Loss estimates and storm science, *WTW Insights*, 2022.
- 1012 Screen, J. A., Eade, R., Smith, D. M., Thomson, S., and Yu, H.: Net Equatorward Shift of the Jet Streams When  
1013 the Contribution From Sea-Ice Loss Is Constrained by Observed Eddy Feedback, *Geophys. Res. Lett.*, 49,  
1014 e2022GL100523, <https://doi.org/10.1029/2022GL100523>, 2022.
- 1015 Serinaldi, F. and Papalexiou, S. M.: Random fields simplified: Preserving marginal distributions, correlations,  
1016 and intermittency, with applications from rainfall to humidity., *Water Resour. Res.*, 56, e2019WR026331, 2020.
- 1017 Serinaldi, F., Lombardo, F., and Kilsby, C. G.: Testing tests before testing data: an untold tale of compound  
1018 events and binary dependence, *Stochastic Environmental Research and Risk Assessment*, 36, 1373–1395,  
1019 <https://doi.org/10.1007/s00477-022-02190-6>, 2022.
- 1020 Siegmund, J. F., Siegmund, N., and Donner, R. V.: CoinCalc—A new R package for quantifying simultaneities of  
1021 event series, *Computers and Geosciences*, 98, 64–72, <https://doi.org/10.1016/j.cageo.2016.10.004>, 2017.
- 1022 Simpson, N. P., Mach, K. J., Constable, A., Hess, J., Hogarth, R., Howden, M., Lawrence, J., Lempert, R. J.,  
1023 Muccione, V., Mackey, B., New, M. G., O’Neill, B., Otto, F., Portner, H.-O., Reisinger, A., Roberts, D., Schmidt, D.  
1024 N., Seneviratne, S., Strongin, S., van Aalst, M., Totin, E., and Trisos, C. H.: A framework for complex climate  
1025 change risk assessment, *One Earth*, 4, 489–501, <https://doi.org/10.1016/j.oneear.2021.03.005>, 2021.
- 1026 Smith, K. and Phillips, I. D.: Autumn and Extended Winter Daily Precipitation Variability over Central and  
1027 Southern Scotland, *Scottish Geographical Journal*, 128, 42–63, <https://doi.org/10.1080/14702541.2012.691337>,  
1028 2012.
- 1029 Southern, R. L.: The global socio-economic impact of tropical cyclones., *Aust. Meteorol. Mag.*, 27, 175–195,  
1030 1979.
- 1031 Stalhandske, Z., Steinmann, C. B., Meiler, S., Sauer, I. J., Vogt, T., Bresch, D. N., and Kropf, C. M.: Global multi-  
1032 hazard risk assessment in a changing climate, *Scientific Reports*, 14, 5875, <https://doi.org/10.1038/s41598-024-55775-2>, 2024.

- 1034 Stephan, C. C., Ng, Y. H., and Klingaman, N. P.: On Northern Hemisphere Wave Patterns Associated with Winter  
1035 Rainfall Events in China, *Advances in Atmospheric Sciences*, 35, 1021–1034, [https://doi.org/10.1007/s00376-](https://doi.org/10.1007/s00376-018-7267-7)  
1036 018-7267-7, 2018.
- 1037 Tian, X., Schleiss, M., Bouwens, C., and van de Giesen, N.: Critical rainfall thresholds for urban pluvial flooding  
1038 inferred from citizen observations, *Science of the total environment*, 258–268,  
1039 <https://doi.org/10.1016/j.scitotenv.2019.06.355>, 2019.
- 1040 Tucker, S. O., Kendon, E. J., Bellouin, N., Buonomo, E., Johnson, B., and Murphy, J. M.: Evaluation of a new 12  
1041 km regional perturbed parameter ensemble over Europe, *Clim. Dynam.*, 58, 879–903,  
1042 <https://doi.org/10.1007/s00382-021-05941-3>, 2022.
- 1043 UNEP: Agenda 21. Tech. rep., United Nations Environment Programme, 1992.
- 1044 Vignotto, E., Engelke, S., and Zscheischler, J.: Clustering bivariate dependencies of compound precipitation and  
1045 wind extremes over Great Britain and Ireland., *Weather Clim. Extremes*, 32, 100318, 2021.
- 1046 Vitolo, R., Stephenson, D. S., Cook, I., and Mitchell-Wallace, K.: Serial clustering of intense European storms,  
1047 *Meteorologische Zeitschrift*, 18, 411–424, <https://doi.org/10.1127/0941-2948/2009/0393>, 2009.
- 1048 Volonté, A., Gray, S. L., Clark, P. A., Martínez-Alvarado, O., and Ackerley, D.: Strong surface winds in Storm  
1049 Eunice. Part 1: storm overview and indications of sting jet activity from observations and model data, *Weather*,  
1050 78, <https://doi.org/10.1002/wea.4402>, 2023a.
- 1051 Volonté, A., Gray, S. L., Clark, P. A., Martínez-Alvarado, O., and Ackerley, D.: Strong surface winds in Storm  
1052 Eunice. Part 2: airstream analysis, *Weather*, 78, <https://doi.org/10.1002/wea.4401>, 2023b.
- 1053 Ward, P. J., Daniell, J. E., Duncan, M., Dunne, A., Hananel, C., Hochrainer-Stigler, S., Tijssen, A., and Torresan, S.:  
1054 Invited perspectives: A research agenda towards disaster risk management pathways in multi-(hazard-)risk  
1055 assessment, *Natural Hazards and Earth System Science*, 22, 1487–1497, [https://doi.org/10.5194/nhess-22-](https://doi.org/10.5194/nhess-22-1487-2022)  
1056 1487-2022, 2022.
- 1057 White, A. U.: Natural hazards, local, national, global, in: *Natural hazards, local, national, global*, edited by:  
1058 Gilbert, G. F., Oxford University Press, New York, 288, 1974.
- 1059 Wilkinson, S., Dunn, S., Adams, R., Kirschner-Bossi, N., Fowler, H., Otálora, S., Pritchard, D., Mednes, J., Palin, E.,  
1060 and Chan, S.: Consequence forecasting: A rational framework for predicting the consequences of approaching  
1061 storms, *Climate Risk Management*, 35, 100412, <https://doi.org/10.1016/j.crm.2022.100412>, 2022.
- 1062 Williams, G. P.: Bank-full discharge of rivers, *Water Resour. Res.*, 14, 1141–1154, 1978.
- 1063 Woolings, T., Hannachi, A., and Hoskins, B.: Variability of the North Atlantic eddy-driven jet stream, *Q. J. R.*  
1064 *Meteorol. Soc.*, 856–868, <https://doi.org/10.1002/qj.625>, 2010.
- 1065 Woolings, T., Drouard, M., O’Reilly, C. H., Sexton, D. M. H., and McSweeney, C.: Trends in the atmospheric jet  
1066 streams are emerging in observations and could be linked to tropical warming, *Communications Earth and*  
1067 *Environment*, 4, 125, <https://doi.org/10.1038/s43247-023-00792-8>, 2023.
- 1068 Zappa, G., Pithan, S., and Shepherd, T.: Multimodel evidence for an atmospheric circulation response to Arctic  
1069 sea ice loss in the CMIP5 future projections, *Geophysical Research Letters*, 54, 1011–1019,  
1070 <https://doi.org/10.1002/2017GL076096>, 2018.
- 1071 Zscheischler, J. and Seneviratne, S. I.: Dependence of drivers affects risks associated with compound events,  
1072 *Science Advances*, 3, e1700263, 2017.

1073 Zscheischler, J., Westra, S., van der Hurk, B. J. J. M., Seneviratne, S. I., Ward, P. J., Pitman, A., AghaKouchak, A.,  
1074 Bresch, D. N., Leonard, M., Wahl, T., and Zhang, X.: Future climate risk from compound events, *Nature Climate*  
1075 *Change*, 8, 469–477, <https://doi.org/10.1038/s41558-018-0156-3>, 2018.

1076 Zscheischler, J., Naveau, P., Martius, O., Engelke, S., and Raible, C. C.: Evaluating the dependence structure of  
1077 compound precipitation and wind speed extremes, *Earth System Dynamics*, 12, 1–16,  
1078 <https://doi.org/10.5194/esd-12-1-2021>, 2021.

1079

## 1080 **Appendix A: Event Sets**

1081

### 1082 *A.1 Dataset selection & fields used*

1083

1084 This study uses the UK Climate Projections 2018 (UKCP18) regional simulations. On a 12 km grid, over the  
1085 commonly used EURO-CORDEX domain (Jacob et al., 2014), simulations were run from 1980–2080 using the  
1086 Representative Concentration Pathway (RCP) 8.5 climate change scenario with 12 member perturbed  
1087 parameter ensemble (Tucker, et al., 2022). Hourly 10m instantaneous wind gusts and total precipitation were  
1088 available from the 12 ensemble members for two periods (1981–2000, 2061–2080), and UKCP18-based river  
1089 flows for these two time periods have been derived (Griffin et al., 2022b) by using the simulated precipitation  
1090 and temperature, and derived evapotranspiration, to drive the Grid-to-Grid (G2G) hydrological model (Kay et  
1091 al., 2021). From these daily mean river flows output by G2G on a 1 km grid over GB, a set of high-flow events  
1092 was created and is openly available (Griffin et al., 2022a). A daily time-series of the area subject to extreme  
1093 high flows was also provided to the authors.

1094

1095 Thus, UKCP18 is selected as it presents the opportunity for more extreme wind and high-flow events to be  
1096 analysed than in the observational record, and for future changes to be examined. The UKCP18 simulations are  
1097 argued to well represent extreme precipitation (Cotterill et al., 2021; Lane and Kay, 2021; Lowe et al., 2018;  
1098 Tucker, et al., 2022) and wind gusts (Manning et al., 2023) when assessed against lower resolution climate  
1099 model simulations and gridded historical observations. Importantly, rank correlation between GB aggregated  
1100 precipitation, high-flows and extreme wind for the simulated present (1981-2000) closely matches the ~30 km  
1101 resolution ERA5 reanalysis (1979-2021)(Hersbach et al., 2020) and GLOFAS river-flows derived from it using  
1102 LISFLOOD (Harrigan et al., 2023; Hirpa et al., 2018) across time windows from 1 to 180 days (Bloomfield et al.,  
1103 2023). In other words, even after higher-resolution verification (i.e. against CAMELS-GB/CHESS-MET), the  
1104 UKCP18 simulations appear to adequately capture co-occurrence of the extreme wind and high flows  
1105 (Bloomfield et al., 2023, 2024).

1106

### 1107 *A.2 Defining widespread hazard-specific events*

1108

1109 For the present time period, 1981–1999, UKCP18 has 19 complete extended winters over 12 ensemble  
1110 members, giving 228 simulated seasons designated here by the year they start in (i.e. Oct 1981 – Mar 1982 is  
1111 ‘1981’). These contain unrealised yet plausible extremes. Griffin et al. (2022a, b) used the 99.5<sup>th</sup> percentile of  
1112 flow across the *whole* year ( $q_{i,j}^{99.5}$ , Jan-Dec) and required that greater than 0.1% of the area of the GB river  
1113 network (19,914 grid cells, ~20 km<sup>2</sup>) exceed its threshold to constitute being within an event (blue shaded  
1114 areas in Fig. 2). In addition a 14-day maximum event length was imposed, and events sub-divided if flow

1115 dropped to under 1/3 of the lowest of two included peaks which were separated by at least an estimated time-  
 1116 to-peak of storm hydrographs. This is a point-over-threshold approach (e.g., Lechner et al., 1993; Robson and  
 1117 Reed, 1999) and their intention was to isolate hydrologically independent, extreme and widespread events.  
 1118 Here, matching sets of events for extreme wind, and for completeness precipitation, are extracted.

1119  
 1120 Grids of daily totals of precipitation ( $p$ ) and maximum 10m wind gust ( $v$ ) are created, and used to define events  
 1121 ( $E$ ). Each event is the spatial footprint of the maxima driving that hazard (e.g.  $v$ ) over a time-window  
 1122 containing an isolated hydro-meteorological extreme.

1123  
 1124 For wind events, a daily time series for  $v$  of the areal fraction of GB where it exceeds its grid cell's 98<sup>th</sup>  
 1125 percentile ( $v_{i,j}^{98}$ , Oct-Mar) is first computed (Fig. 2). Then, the temporal limits ( $t_{start}$  and  $t_{end}$ ) of the extreme  
 1126 event days are defined as the first and last day of a period where this areal fraction is at least 0.1% of the whole  
 1127 GB land area (~300 km<sup>2</sup>). 0.1% is used for consistency with flooding (Griffin et al., 2022a), and the 98<sup>th</sup>  
 1128 percentile aligns with a recent consensus for wind impact estimation (e.g., Bloomfield et al., 2024; Klawns and  
 1129 Ulbrich, 2003; Priestley et al., 2018) outlined in Appendix A.3. Thus, based on these thresholds, each event  
 1130 consists of a sequence of consecutive extreme days, with the maximum windspeed ( $v$ ) across the duration of  
 1131 the event retained at each location to give an event its footprint. No wind event ever exceeds 8 days ( $95\% \leq 3$   
 1132 days, Fig. A1), so the limit of 14 days used by Griffin et al (2022b, a) is not needed. It is likely that clusters of 2  
 1133 or 3 meteorologically distinct cyclonic systems (Mailier et al., 2006; Priestley et al., 2018; Vitolo et al., 2009)  
 1134 combine within longer wind events. However, the focus here is on periods of disruption as they are  
 1135 experienced.

1136  
 1137 Precipitation events footprints are created exactly as for wind, except that the sum of precipitation ( $p$ ) across  
 1138 the duration of the event is retained at each location (i.e. instead of the maximum).

1139  
 1140  
 1141 *Table 2: Table of thresholds or limits used to define events. These thresholds used (i) in defining events and (ii) calculating severity indices*  
 1142 *are not to be confused with the percentiles used to distinguish events of differing severity in the Results (e.g. 75<sup>th</sup> percentile of events*  
 1143 *once they have been isolated and quantified in terms of a severity index).*

Threshold / Limit	Value
Percent of river network ( $q$ )	0.1%
Percent of GB land area ( $v, p$ )	0.1%
Extreme peak river flow (whole year), percentile of daily values.	99.5%

Extreme precipitation (Oct-Mar), percentile of daily values.	98.0%
Extreme daily 10 m max wind gust (Oct-Mar), percentile of daily values.	98.0%
Maximum length of event - from Griffin et al (2022a)	14 days

1144

### 1145 A.3 Event severity indices

1146

1147 Severity indices are ‘impact-based proxies’ for hazards such as flooding and wind extremes (Hillier and Dixon,  
1148 2020), calibrated against and designed to reflected potential damage (Bloomfield et al., 2023; e.g., Christofides  
1149 et al., 1992; Heneka and Ruck, 2008; Hillier and Dixon, 2020; Klawa and Ulbrich, 2003).

1150

1151 Storm Severity Indices (SSI) aim to condense the risk associated with a wind event into a single number  
1152 incorporating factors thought to drive damage such as maximum wind gust ( $v$ ), area affected and duration  
1153 (e.g., Christofides et al., 1992; Dorland et al., 1999; Klawa and Ulbrich, 2003). Recently, following Klawa and  
1154 Ulrich (2003) a form of SSI using  $v^3$  in excess of a 98<sup>th</sup> percentile minimum threshold beneath which no  
1155 damage occurs has become well-established as a norm (Bloomfield et al., 2023; e.g., Leckebusch et al., 2008;  
1156 Osinski et al., 2016; Priestley et al., 2018). Rather than a region defined by a simple (e.g. circular) geometry  
1157 (Manning et al., 2022, 2024), grid cells over land (e.g., Bloomfield et al., 2023; Pinto et al., 2012) are used to  
1158 represent GB impact. For simplicity and to avoid a judgement linking value directly to population density (e.g.  
1159 consider a wind farm), in contrast to Bloomfield et al. (2023), no population weighting is used. Thus, each  
1160 event’s severity  $SSI(E)$  is given by Eq. (1):

1161

$$1162 \quad SSI(E) = \sum_{i=1}^{N_i} \sum_{j=1}^{N_j} \left( \frac{v(E)_{i,j}}{v_{i,j}^{98}} - 1 \right)^3 \cdot I_{i,j}$$

1163

$$I_{i,j} = \begin{cases} 0 & \text{if } v(E)_{i,j} < v_{i,j}^{98} \\ 1 & \text{otherwise} \end{cases}$$

1164

1165 Two types of model have been used to approximate loss ( $l$ ) or SSI, power-law ( $l = k_1 v^\alpha$  for  $v > v_{\text{thresh}}$ ) and  
1166 exponential ( $l = k_2 e^{\beta v}$ ), where  $k_1$ ,  $k_2$ ,  $\alpha$  and  $\beta$  are constants, parameters to be determined by fitting to loss  
1167 data. In general, the challenge is to approximate data where losses rise steeply above  $\sim 32\text{ms}^{-1}$  (Christofides et  
1168 al., 1992; Dorland et al., 1999; Heneka and Ruck, 2008). Using no threshold an exponential form, which can rise  
1169 very abruptly, fits postcode district losses for 5 storms better than  $\alpha$  of 2-4 (Dorland et al., 1999). With a  
1170 threshold of  $\sim 20\text{-}24\text{ms}^{-1}$  or the 98<sup>th</sup> percentile (e.g., Christofides et al., 1992; Klawa and Ulbrich, 2003)  $v^3$  can  
1171 fit losses for a storm (i.e. within 1-2 days) at district or national resolution, and allow modelling of district level

1172 historical losses (e.g., Pinto et al., 2012). This said, the 1999 storms sequence (Anatol, Lothar, Martin) showed  
1173 losses above  $24 \text{ ms}^{-1}$  may on occasion rise more sharply for certain domains (i.e.  $v^4 - v^5$  for Denmark,  
1174 Germany)(MunichRe, 2002).

1175  
1176 At a daily timescale a 98<sup>th</sup> percentile threshold (i.e.  $\sim 7$  times per year) arises as, in practice, relatively little  
1177 damage occurs below this level ( $\sim 20 \text{ ms}^{-1}$ ) in the flat areas of UK and German (Klawe and Ulbrich, 2003;  
1178 Palutikof and Skellern, 1991). Of course some places, such as mountains, are windier (Heneka et al., 2006; e.g.,  
1179 Hewston and Dorling, 2011) but both nature (e.g. trees) and the built environment appear to adapt to this  
1180 recurrence level. Klawe and Ulbrich (2003) illustratively note that winds at List (island of Sylt) exceed  $20 \text{ ms}^{-1}$  1-  
1181 in-5 days to no noticeable detriment, and building regulations (e.g. UK, Germany, Netherlands) require greater  
1182 resilience in windier areas (e.g., Böllman and Jurksch, 1984; Chandler et al., 2001; Dorland et al., 1999; Hill et  
1183 al., 2013). Whilst a higher percentile might be appropriate for higher frequency data (6-hourly, 99<sup>th</sup>) (Manning  
1184 et al., 2024), damage on 2% of days (i.e. 98<sup>th</sup> percentile) is not wildly different from the number of UK storms,  
1185 which are named (i.e. 7-8 per/year) when the Met Office believes it has '*potential to cause disruption or*  
1186 *damage*' (Met Office, 2024).

1187  
1188 Probabilistic models account for the uncertainty in how individual assets are damaged (Heneka et al., 2006;  
1189 Heneka and Ruck, 2008), for instance using a power-law and replacing the threshold with a function describing  
1190 the probability of damage (Pardowitz et al., 2016; Prahel et al., 2012). This better approximates losses in  
1191 Germany across all 2004 wintertime days in 11 years (1997-2007), although the costliest days ( $\sim 10$  per year)  
1192 are still adequately modelled using cubic excess-over-threshold approach with a 98<sup>th</sup> percentile (Prahel et al.,  
1193 2015). Thus using Eq. (1) is appropriate as these 'extremes' are the focus of this paper, particularly as ranks  
1194 rather than absolute SSI values are primarily evaluated. Moreover, sensitivity testing indicates limited  
1195 sensitivity of patterns of correlation (e.g. spatial) to are largely choice of threshold (Hillier and Dixon, 2020),  
1196 something borne out by the convergence of results for recent UK flood-wind research that have employed a  
1197 spectrum of methodological choices (see Section 4.1).

1198  
1199 Storm duration has been argued to influence losses (e.g., Christofides et al., 1992), but statistical studies have  
1200 found that it does not improve models and may risk 'over-fitting' (Dorland et al., 1999), so in line with the  
1201 Klawe and Ulbrich (2003) such potential influences (e.g. precipitation, duration) are not included here. We  
1202 also note that  $v^3$  is theoretically related to kinetic energy flux (e.g., Pinto et al., 2012) and to the dissipation of  
1203 kinetic energy in the surface layers of a storm (Bister and Emanuel, 1998; Businger and Businger, 2001;  
1204 Emanuel, 1998, 2005). However, we discount this as any justification for a cubic relationship between  
1205 economic loss and  $v$ , other than perhaps as for the presence of non-linearity. Simply, for cubically increasing  
1206 losses over a threshold (e.g., Christofides et al., 1992; Dorland et al., 1999) a cubic relationship that starts at  
1207 zero velocity, as kinetic energy must, does not fit them well (Prahel et al., 2015).

1208

1209 Based on the form of SSI, Flood Severity Indices (FSI) have recently been developed (Bloomfield et al., 2023,  
1210 2024). Only grid cells on the river network (e.g., Bloomfield et al., 2023) are used, again with no population  
1211 weighting. Thus, each events' flood severity  $FSI(E)$  is given by Eq. 2:

1212

1213

$$FSI(E) = \sum_{i=1}^{N_i} \sum_{j=1}^{N_j} \left( \frac{q(E)_{i,j}}{q_{i,j}^{99.5}} - 1 \right) \cdot I_{i,j}$$

1214

$$I_{i,j} = \begin{cases} 0 & \text{if } q(E)_{i,j} < q_{i,j}^{99.5} \\ 1 & \text{otherwise} \end{cases}$$

1215

1216 The 99.5<sup>th</sup> percentile is inherited, for consistency, from Griffin et al (2022a). It is largely arbitrary, intended to  
1217 yield sufficient data points for statistical analysis (Bloomfield et al., 2023; Griffin et al., 2022b). It is less than the  
1218 2-year return period 'rule of thumb' for bank-full discharge (i.e. 99.9<sup>th</sup> percentile), although the work this  
1219 derives from (Williams, 1978) is highly equivocal (i.e. 1-32 year range) due to factors such as basin  
1220 characteristics, local climate and flood defences (Berghuijs et al., 2019; e.g., Tian et al., 2019). The cubic power  
1221 is removed as it is not required with, as for SSI, justification of this functional form of FSI being through  
1222 validation, replicating losses and capturing known floods (Bloomfield et al., 2023). Historical FSIs are highly  
1223 correlated ( $r = 0.74$ ,  $p < 0.05$ ) with infrastructure loss data on an annual timescale, and FSI captures 28 of 34  
1224 wintertime floods (1980-2020) in the Chronology of British Hydrological Events (Black and Law, 2004). This said,  
1225 lots of small FSI 'events' occur where no flooding was historically recorded. Also, without a threshold non-  
1226 linearity (i.e.  $SI \sim^5$ ) improves the fit of one proxy to losses (Hillier and Dixon, 2020), so debate on the form of  
1227 FSI is expected to continue.

1228

1229 FSI as configured in Eq. 2 is suitable here as only the most extreme events are selected (i.e. >75<sup>th</sup> percentile of  
1230 events). This is 5-6 high flows per year, comparable to the ~7 floods per year in commercial risk models (Hillier  
1231 et al., 2024).

1232

1233 A Precipitation Severity Index (PSI) is used for consistency, despite severity perhaps being an incorrect term as  
1234 rain itself rarely does damage directly (Manning et al., 2024). PSI is defined as for SSI, except that a cubic  
1235 relationship is omitted as there is no justification for the additional complexity.  $PSI(E)$  for each event is given by  
1236 Eq. 3:

1237

1238

$$PSI(E) = \sum_{i=1}^{N_i} \sum_{j=1}^{N_j} \left( \frac{p(E)_{i,j}}{p_{i,j}^{98}} - 1 \right) \cdot I_{i,j}$$

$$I_{i,j} = \begin{cases} 0 & \text{if } p(E)_{i,j} < p_{i,j}^{98} \\ 1 & \text{otherwise} \end{cases}$$

1239  
1240  
1241  
1242  
1243  
1244  
1245  
1246  
1247  
1248  
1249  
1250  
1251  
1252  
1253  
1254  
1255  
1256  
1257  
1258  
1259  
1260  
1261  
1262  
1263  
1264  
1265  
1266  
1267  
1268  
1269  
1270  
1271  
1272  
1273

#### A.4 Description of Event Sets

A set of high-flows events (Griffin et al., 2022b, a) has been created for the UKCP18 12-member perturbed parameter ensemble (PPE) of the Hadley Centre 12km Regional Climate Model (RCM) (Murphy et al., 2019; Tucker, et al., 2022). Thus, to mirror this, UKCP18 was used to generate wind ( $n = 3,427$ ) and precipitation ( $n = 14,502$ ) events across mainland Great Britain for baseline (winters 1981-1999) and future (winters 2061-2079) time-slices. The wind event set is broadly aligned to other such sets in its construction methods (Lockwood et al., 2022; Osinski et al., 2016; Roberts et al., 2014), and the data been validated for the purposes of examining hazard co-occurrence (Appendix A.1). Summary metrics are created for these event footprints (total area, duration, SI) and assigned to a single date  $t_{max}$ , the individual day when the greatest number of grid cells exceed the set threshold.

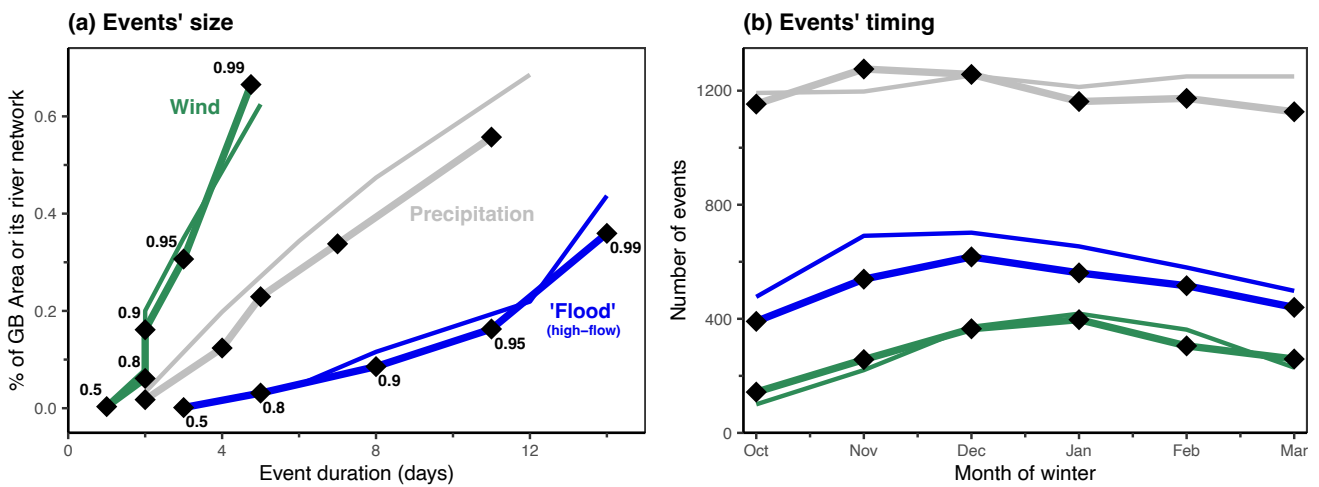
First consider the size and number of events at the present time. There are 7-8 wind events per year in 1981-1999 on average, each tending to affect a large area (i.e. up to 60% of GB) but be relatively short-lived (< 5-day). This contrasts longer-duration yet more localized fluvial flooding (Fig. A1a). These properties match what is typical of these event types (e.g. Mitchell-Wallace et al., 2017). No wind event ever exceeds 8 days, so the limit of 14 days used by Griffin et al (2022b, a) is not needed. Extreme precipitation is more common than wind with 31-33 events per year, as is flooding at 13-16 events per year.

The relative frequency of events is statistically dictated, depending upon the size of each phenomenon and the parameters (e.g. thresholds) used to extract events. The spatial length-scale of correlation (i.e. floods are typically smaller) increases their number, counteracted somewhat by them lasting longer and the higher percentile. Imagine an idealised scenario wherein windstorms hit the whole UK, whilst floods impact 10% of its area (e.g. in 10 uncorrelated areas). Now, for a 98<sup>th</sup> daily percentile, every 1 in 50 days all WS points will peak at the same time giving 1 event. For flood, this will happen separately in the 10 areas, giving 10 events. The higher percentile (i.e. 99.5<sup>th</sup> vs 98<sup>th</sup>) used for flooding will reduce this by four times, giving 2.5 events in 50 days. Also, by lasting longer, the flood events might merge more readily, reducing their number.

The events in 2061-2079 have some differences to 1981-1999. Fig. A1 echoes the finding of Griffin et al (2022b) that flooding is expected to be more frequent (+18% here) and heavier tailed with larger extreme events (Fig. A1a) and somewhat more seasonal with a focus in mid-winter (DJF), but also identifies a potential shift to a slightly earlier peak in future (Fig. A1b). Considering all events, neither precipitation nor wind events increase in number significantly into the future ( $t$ -test between means of ensemble members), and echoes the

1274 muted changes in climatology (e.g., Manning et al., 2022, 2024). It differs, however, from true extremes are  
 1275 examined in papers (Bloomfield et al., 2023) or the main text. Illustratively, increases for Oct-Mar are +59% for  
 1276 the 75<sup>th</sup> percentile of FSI, +91% for the 95<sup>th</sup> percentile of FSI in Fig. 6a,d, both of which are significant ( $p < 0.01$ ).  
 1277

1278 Only the top quarter of events defined are focussed upon (i.e. most severe quarter, >75<sup>th</sup> percentile). For wind  
 1279 events there are 7-8 per year in total, which roughly reflects the Met Office's named storms 2015-2023  
 1280 (7.4/yr)(Met Office, 2024). Thus, 1-2 per year are focussed upon, comparable to the ~3 per year used in  
 1281 insurance industry risk modelling (Hillier et al., 2024). There are 15 high flow events per year, and taking the  
 1282 top quarter gives ~4 notable high-flow events, comparable to the 6-7 floods per year in a commercial model  
 1283 (Hillier et al., 2024).  
 1284



1285  
 1286  
 1287 *Fig. A1: (a) Size and duration of events created for Wind, Precipitation and Flood. 'Flood' events are high-flow events created by Griffin*  
 1288 *et al (2023). Percentiles are shown from 50th to 99th, calculated separately for duration and area (i.e. this is not a joint distribution).*  
 1289 *Present day (thick lines) and future (thin lines) are similar if all the events are considered. (b) Seasonality of the events.*